Simulation of nano-scale flows by molecular dynamics methods

A Thesis
Submitted for the Degree of
MASTER OF SCIENCE (ENGINEERING)
in the Faculty of Engineering

By

Antina Ghosh

ENGINEERING MECHANICS UNIT
JAWAHARLAL NEHRU CENTRE FOR ADVANCED SCIENTIFIC
RESEARCH
Bangalore - 560 064
JANUARY 2005

To my father

DECLARATION

I hereby declare that the matter embodied in the thesis entitled "**Simulation of nano-scale flows by molecular dynamics methods**" is the result of investigations carried out by me at the Engineering Mechanics Unit, Jawaharlal Nehru Centre for Advanced Scientific Research, Bangalore, India under the supervision of Prof. Rama Govindarajan and Prof. Srikanth Sastry and that it has not been submitted elsewhere for the award of any degree or diploma.

In keeping with the general practice in reporting scientific observations, due acknowledgement has been made whenever the work described is based on the findings of other investigators.

Antina Ghosh

CERTIFICATE

We hereby certify that the matter embodied in this thesis entitled "**Simulation of nano-scale flows by molecular dynamics methods**" has been carried out by Ms. Antina Ghosh at the Engineering Mechanics Unit, Jawaharlal Nehru Centre for Advanced Scientific Research, Bangalore, India under our supervision and that it has not been submitted elsewhere for the award of any degree or diploma.

Prof. Rama Govindarajan
(Research Supervisor)

Prof. Srikanth Sastry
(Research Supervisor)

Acknowledgements

When I stop for a moment and look back at the days past, I see many faces that have influenced my life in different ways and helped me grow to this stage. I am happy to express my gratitude to all of them.

I would like to thank my supervisors Prof. Rama Govindarajan and Prof. Srikanth Sastry for their guidance and suggestions that led to the successful completion of the present thesis. My interactions with Prof. Govindarajan have improved my concepts in fluid mechanics. She has taught me to look at even the smallest details of a problem critically. I am grateful to her for her support at different points of time during the last two years. I am thankful to Prof. Sastry for his generous time and all the discussions that led to a better understanding of the problem and helped me learn different aspects of the field in detail. My working experience with him has trained me to be independent, which is an essential ingredient of a researcher. I want to thank him especially for the book grant that enabled me to buy some of the books that I had yearned to possess.

I wish to thank the chairman of our unit, Prof. Narasimha, the little interactions with him always encouraged me.

My interactions with Dr. Umesh Waghmare was mainly through a course work on Computational methods. He is a good teacher and a nice person to know. I am grateful to him for his support and encouragement in my research.

I am indebted to all my teachers at the Calcutta University for the things they taught me and in particular for their care and concern.

The support and encouragement of my family have always helped me to move forward through all the phases of life. I owe to my father for every little thing I learnt from him. He is the first person to help me in knowing different shades of life and made me realise that it is not a 'pond', but a 'sea'. His advices, encouraging words and actions influenced me to a great extent and determined the direction of my life. The struggles of his life and his never-say-die spirit have always given me the courage at all my difficult times.

My mother's love, care and patience are the resting places for me all the time. She has always given me the freedom to do things the way I liked to. I thank Bubun, my brother, for sharing all his poems with me. Listening to his poems and recitations is indeed a beautiful experience. Vijay has made a difference in my life with his care, understanding and support. I am happy to appreciate all the efforts he has taken to keep me on the right track.

It is a pleasure to write about my friends - it reminds me of all those delightful moments I shared with them. Suranjana, Shrabana, Indranil, Utpal, Sumana, Rajarshe and many others, with whom I spent a wonderful time at Calcutta University. Especially, the memories of our trip to Pelling are unforgettable. Sathi has been my long time friend since college days. Her affection, friendship and sharing are assets for me. Anindyada, Apu, Rikun, Sona - their friendship and company have added colours to my life.

I will always remember the sharing and warmth that I have received from many of my friends and batchmates at JNC. Prasenjit, Joydeep, Shibu, Moumita Saharay, Kavitha, Ayan, Mousumi, Debu, Bhaswati and many others helped me in different ways and the moments I shared with them made my life enjoyable at JNC. Krishnan helped me in clarifying many doubts during the intial stages of my research work. He always welcomed my questions and helped me as far he could. I wish to thank my labmates Vinod, Sameen, Pinaki, Shreyas, Kaushik and others for their co-operation and help, which were essential at different stages of my work. I thank Rajesh Kanna who was always ready to extend a helping hand in computer related matters.

The time I have spent at this shrine of science has given me a lot. My decision to pursue science after postgraduation was just an option. But JNC has made this option an aim. All my experiences and interactions at JNC not only helped me to decide my future ways, but also helped me to mature as a person.

Synopsis

The density variation and the driven flow of a model liquid interacting via 12-6 Lennard Jones potential in a nano-sized channel has been studied through molecular dynamics simulations. The channel is unbounded in x and y directions through the use of periodic boundary condition and in the z direction it is bounded by walls (lying in the x-y plane) on both sides and the separation between the walls is of the order of nanometers. Two types of wall have been studied - a smooth structureless wall and an atomic wall. The smooth wall is modelled by a Lennard Jones 10-4 potential. The atomic wall is composed of layers having 001 fcc structure with wall atoms interacting with each other through the Lennard Jones 12-6 potential of strength six times that of the fluid-fluid interaction strength. Simulations are done for both static and moving wall atoms. In the first case, wall atoms are assumed to have infinite mass and therefore remain static at their original position throughout the simulation. In the second case, wall atoms have finite mass and are allowed to move about their mean position. The density variation across the channel is computed with the static wall. The simulated density profile is compared with Koplik & Banavar (1988) and found to match very well. A Poiseuille flow is simulated in the same system by imposing a constant body force along the x direction on each fluid atom. The flow is simulated over a range of the body force for which thermal equilibrium exists between the wall and the fluid system. The simulated profiles at different body force are fitted with Stokes profiles and viscosity values are estimated from the fitting parameters. The viscosity values obtained from the present simulation lie within the range estimated by Koplik & Banavar (1988). The shear viscosity of the bulk liquid is calculated independently by non-equilibrium molecular dynamics methods which yield viscosity values consistent with the estimates from fitting the velocity profiles.

List of Figures

List of Tables

Contents

CHAPTER 1

Introduction

1.1 Nanoscience

Nanoscience is associated with novel physical, chemical and biological phenomena at size scales ranging from individual molecules or atoms to micrometers. There has been rapid progress in this area due to its wide range of possible technological applications. Research work at the nanoscale in industries is mainly driven by miniaturization in electro-mechanical devices eg. micro or nano pumps, actuators, valves and sensors. Emerging technology has propelled a strong interest in understanding the physics involved.

A typical example of such small scale systems is a fluid confined in a pore or slit of diameter or height of the order of nanometers. Many effects, such as surface effects which are otherwise negligible become dominant. Consequently there can be differences in flow behavior which we would like to study.

1.2 Why simulation?

The flow field at macroscopic lengthscales can be described by a set of differential equations (Navier Stokes and continuity) but it is difficult to formulate

1

general theoretical equations which cover all the effects that become dominant at small scales. Even if any such theory is formulated, often many microscopic effects are neglected and consequently understanding remains incomplete. Another way of exploring this domain is by doing experiment, which is often difficult due to the complexity, expense, and possible hazards involved. The use of numerical techniques to analyze problems at this scale have the advantage that many-body effects present in the system can be taken into account explicitly through the direct calculation of the interactions between different entities of the system. Numerical methods not only provide efficient benchmarks for theoretical models but can also address details of complex phenomena that can be difficult in theory as well as in experiment. The results of numerical techniques are however subject to uncertainties that arise from *e.g.* the interaction potential model and the numerical schemes used.

1.3   Previous studies

There are several interesting and relatively unexplored flow problems in the micro and nanoscale regime which are equally appealing from the point of view of technology as well as from the stand of basic science. Some examples are the slip of simple liquids over smooth surfaces, gas flows in microchannels, two phase flow in microchannels, microelectrohydrodynamics etc. As discussed in the previous paragraph simulation and experiment are the main tools to study small scale phenomena. The study of flow properties at the microscale started with the study of density variation of fluid near a wall. The first analytical potential that describes the smooth structureless wall and fluid interaction was given by Steele (1973). Abraham (1978) was the first to

study the interfacial density profile of a Lennard Jones fluid in contact with a wall and has considered different types of walls. He used the Lennard Jones 10-4 potential for the structureless wall as given by Steele and also studied the {001} fcc wall, and a Boltzmann weighted wall in their simulation. In the same year Chapela *et al.* (1977) studied the density profile of a gas liquid interface and adsorption properties of a binary mixture through Monte Carlo and molecular dynamics simulations.

The first published work where flow in a microchannel is studied through molecular dynamics simulation is by Koplik & Banavar (1988). They have studied the density structure in a pressure driven channel flow of height of the order of nanometers and boundary conditions for moving contact lines in their simulation. They used an atomic wall with fcc {001} structure and assumed highly massive wall atoms, so that they remain essentially static at their lattice sites throughout the simulation. They have done the simulation for a range of densities starting from typical liquid density 0.8 (in reduced units) up to 0.08. They observed the validity of the no-slip boundary condition up to the density 0.6 and a smooth transition to slip at lower densities. Thompson & Robbins (1990) did a thorough study of Couette flow in a microchannel and of the density profile. They have studied the boundary condition and near-wall density structure with a range of wall-fluid interaction. The effect of different geometries in a pressure driven flow in nanoscale has been discussed in Fan *et al.* (2002). The study of the boundary conditions of a mixture of two viscous liquids flowing past a solid atomic wall was studied by Koplik & Banavar (1989) and they found that velocity of each individual species satisfies the no-slip condition.

An important part of this ongoing research in nanoscale covers the study of the structure, properties and frictional effects of thin films and interfaces. Landmann & Luedtke (1991) have investigated atomistic dynamics of interfacial processes, they have studied films, junctions and nanostructures by molecular dynamics simulation employing realistic interaction potentials. Zhang & Jiang (2003), studied the nanoscale frictional properties between two Si (111) surfaces covered with alkyl monolayers immersed in liquid solvents. A similar system with sheared layer of n-dodacane of thickness of the order of nanometers, confined between two mica surfaces is studied by Cui et al. (2001). They reported the shear rate at which shear thinning takes place in the system under study. The first study of the formation of a jet from a nanosized nozzle is done by Landmann & Luedtke (1991). They have done a thorough study of the condition of formation of the nanojet for different shapes and geometries of the nozzle, stability and break up phenomena by molecular dynamics simulations. They have also modified the lubrication equation adding a Gaussian noise term and their equation gives a well enough match with MD simulation. Eggers (2002) verified Landmann's equation by doing a non-perturbative stability analysis using Landmann's equation and reported similar results.

1.4   Present study

In the present thesis the density variation and the driven flow of a model liquid interacting via 12-6 Lennard Jones potential in a nano-sized channel has been studied through molecular dynamics simulations. The channel is unbounded in x and y directions through the application of periodic boundary condition and in the z direction it is bounded by walls (lying in the x-y

plane) on both sides and the separation between the walls is of the order of nanometers. Two types of wall have been studied - a smooth structureless wall and an atomic wall. The smooth wall is modelled by a Lennard Jones 10-4 potential. The atomic wall is composed of layers having 001 fcc structure with wall atoms interacting with each other through Lennard Jones 12-6 potential of strength six times that of the fluid-fluid interaction strength. Simulations are done for both static and moving wall atoms. In the first case, wall atoms are assumed to have infinite mass and therefore remain static at their original position throughout the simulation. In the second case, wall atoms have finite mass and are allowed to move about their mean position. The density variation across the channel is computed with the static wall. The simulated density profile is compared with Koplik & Banavar (1988) and found to match very well. A Poiseuille flow is simulated in the same system by imposing a constant body force along the x direction on each fluid atom. The flow is simulated over a range of the body force for which thermal equilibrium exists between the wall and the fluid system. The simulated profiles at different body force are fitted with Stokes profiles and viscosity values are estimated from the fitting parameters. The viscosity values obtained from the present simulation lie within the range estimated by Koplik & Banavar (1988). The shear viscosity of the bulk liquid is calculated independently by non-equilibrium molecular dynamics methods which yield viscosity values consistent with the estimates from fitting the velocity profiles.

CHAPTER 2

Molecular Dynamics Method

2.1 Equation of motion for atomic system

Molecular dynamics provides a reasonable physical description of microscale flows predicting all macroscopic averaged properties, hydrodynamics and fluctuations. The equation of motions used to describe particle trajectories are based on the classical Hamiltonian equations given by

$$\dot{p_k} = -\frac{\partial H}{\partial q_k}, \tag{2.1}$$

$$\dot{q_k} = \frac{\partial H}{\partial p_k}, \tag{2.2}$$

where H is the Hamiltonian of the system,

$$H(p,q) = p_k \dot{q_k} - L \ . \tag{2.3}$$

L is the Lagrangian and p_k and q_k are the kth generalized coordinate and momenta respectively. When the potential of the system is independent of velocity and time, kinetic energy is only quadratic in velocity, then the Hamiltonian can be written as

$$H = T + V, \tag{2.4}$$

6

where T is the kinetic energy and V is the potential energy of the system. In Cartesian coordinates Hamilton's equations take the form

$$\dot{p}_k = -\nabla_{r_k} V, \tag{2.5}$$

$$\dot{r}_k = p_k/m \ . \tag{2.6}$$

A system of N interacting particles is described by the above 6N first order differential equations which can be solved with 6N initial conditions to generate the trajectories.

2.2   Discretization

There are a number of numerical schemes which may be used to integrate the above equations of motion. An efficient algorithm is one which ensures reasonable numerical precision at each timestep, low computation time and low storage. One of the most widely used methods is Verlet method (Allen & Tildsley (1987)) which needs only one force calculation per time step. Expanding the position vector in Taylor's series gives,

$$\mathbf{r}(t + \delta t) = \mathbf{r}(t) + \delta t \mathbf{v}(t) + 1/2(\delta t^2)\mathbf{a}(t) + O(\delta t^3), \tag{2.7}$$

$$\mathbf{r}(t - \delta t) = \mathbf{r}(t) - \delta t \mathbf{v}(t) + 1/2(\delta t^2)\mathbf{a}(t) - O(\delta t^3) \ . \tag{2.8}$$

Adding the above two equations we get

$$\mathbf{r}(t + \delta t) = 2\mathbf{r}(t) - \mathbf{r}(t - \delta t) + \delta t^2 \mathbf{a}(t) + O(\delta t^4) \ . \tag{2.9}$$

Also, subtracting 2.8 from 2.7, the velocity is obtained as,

$$\mathbf{v}(t) = [\mathbf{r}(t + \delta t) - \mathbf{r}(t - \delta t))]\,/2\delta t + O(\delta t^2) \ . \qquad (2.10)$$

The accuracy in calculating the position is of the order of $O(\delta t^4)$ whereas the accuracy in estimating the velocity is $O(\delta t^2)$. This algorithm is exactly reversible in time and, given conservative forces, is guaranteed to conserve linear momentum. However, in calculating the position of the atoms a small term $O(\delta t^2)$ is added to a difference of large terms which gives rise to a numerical imprecision at each time step. The velocity in the above scheme is not calculated from direct integration of the equation of motion. For the calculation of the kinetic energy and good temperature control of the system, estimation of velocity needs to be done more accurately. The Verlet scheme is modified to a leap-frog scheme for this purpose. The algorithm is as follows,

$$\mathbf{v}(t + \delta t/2) = \mathbf{v}(t - \delta t/2) + \mathbf{f}/m\delta t + O(\delta t^3). \qquad (2.11)$$

where $\mathbf{f}$ is the force and m is the mass, and the acceleration

$$\mathbf{a} = \mathbf{f}/m \ . \qquad (2.12)$$

The position is updated as

$$\mathbf{r}(t + \delta t) = \mathbf{r}(t) + \mathbf{v}(t + \delta t/2)\delta t + O(\delta t^3) \ . \qquad (2.13)$$

Half step velocities are used to update the position at time t, both the position and velocity updation algorithms are third order accurate.
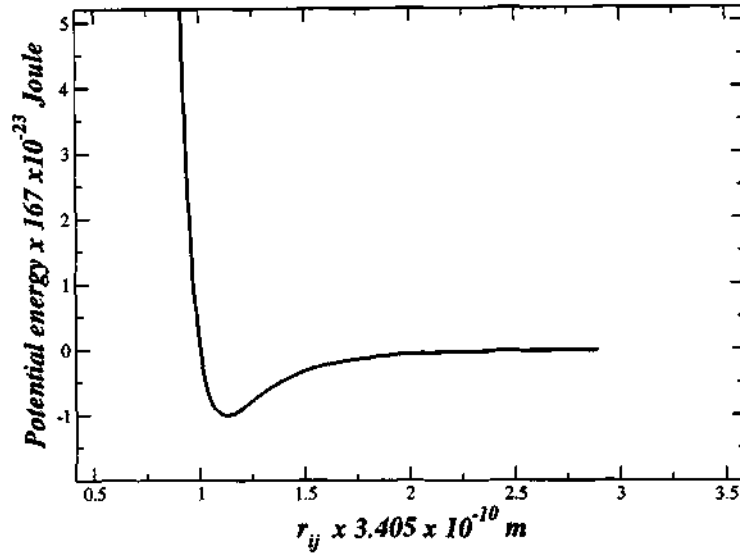
Figure 2.1: 12-6 Lennard-Jones potential.

2.3 Interatomic potential

The interaction between fluid atoms is modelled here by the 12-6 Lennard Jones potential (Allen & Tildsley (1987)) given by

$$V(r) = 4\varepsilon \left[\left(\frac{\sigma}{r_{ij}} \right)^{12} - \left(\frac{\sigma}{r_{ij}} \right)^{6} \right], \qquad (2.14)$$

where ε is the strength of the interaction, σ is the diameter of an atom and r_{ij} is the distance between the ith and j^{th} atom in a liquid. The form of the potential is shown above. The first term models the strong repulsion between two atoms when they come too close to each other and start overlapping. It is an empirical term. The $1/r^{6}$ term describes the weak attractive interaction between the fluid atoms and originates due to the induced dipole-induced dipole interaction that comes into play when two atoms come nearer. The absolute value of the interaction potential at a distance 2.5σ is 1.6% of its well depth. Therefore in calculating the interaction between atoms the cut

off separation is taken as 2.5σ throughout this work. The force acting on the ith particle due to the jth particle is given by

$$\mathbf{F} = -\nabla_i V(r) = 24\epsilon \mathbf{r}_{ij}(1/r_{ij}^2)\left[(\sigma/r_{ij})^{12} - (\sigma/r_{ij})^6\right] \ . \tag{2.15}$$

2.4 Potential model for the smooth wall

A smooth wall can be modelled by a Lennard-Jones 10-4 potential, (Steele (1973)), as a function of the height from the wall. In deriving the potential it is assumed that the atomic centers are continuously distributed over the infinite horizontal plane which makes the wall surface completely structure-less and each wall atom interacts through the Lennard Jones 12-6 potential with the fluid atom. The form of the potential results from the integration over the entire horizontal (xy) plane. The potential felt by a fluid atom due to the presence of a single wall layer at a distance z from the atom is given by

$$V(z) = 2\pi n_s \epsilon \left[2/5(\sigma^{12}/z^{10}) - (\sigma^6/z^4)\right], \tag{2.16}$$

where n_s is the surface density, i.e number of atoms per unit area. The corresponding force is given by

$$F_z = 8\pi n_s \epsilon \left[(\sigma^{12}/z^{11}) - (\sigma^6/z^5)\right] \ . \tag{2.17}$$

The derivation of the 10-4 potential is presented below.

A solid wall is made up of a series of planes along the z direction, where atoms in each of the surface layers are distributed in perfect crystalline order and wall atoms are interacting with the fluid atoms through a 12-6 Lennard-Jones potential. l is a two dimensional lattice vector parallel to this layer

defined as

$$\mathbf{l} = l_1 \mathbf{a}_1 + l_2 \mathbf{a}_2 \ .$$ (2.18)

l_1 and l_2 are integers and $\mathbf{a}_1$ and $\mathbf{a}_2$ are the unit vectors in two dimensions. The periodic surface potential u_s obeys

$$u_s(\mathbf{r} + l) = u_s(\mathbf{r}) \ .$$ (2.19)

The potential $u_s(\mathbf{r})$ can be expressed in a Fourier series in the following way,

$$u_s(\mathbf{r}) = \sum_{g_1,g_2} w_g(z) \exp(i\mathbf{g} \cdot \tau) \ .$$ (2.20)

$\mathbf{r} = (\tau_x, \tau_y, z)$, τ is the two dimensional translational vector and $\mathbf{g}$ is a multiple of reciprocal vectors $\mathbf{b}_1$ and $\mathbf{b}_2$:

$$\mathbf{g} = 2\pi \left[g_1 \mathbf{b}_1 + g_2 \mathbf{b}_2 \right] \ .$$ (2.21)

If we consider a series of planes along z direction, for the αth plane which is at a distance z_α from the fluid atom the above expression can be written as

$$u_s(\mathbf{r}) = \sum_{g_1,g_2} \sum_{\alpha} w_g(z_\alpha) \exp(i\mathbf{g} \cdot \tau),$$ (2.22)

where

$$w_g(z_\alpha) = 1/a_s \int_a \exp(-i\mathbf{g} \cdot \tau) u_s(z_\alpha, \tau) \ .$$ (2.23)

Now the potential at any point $\mathbf{r}$ (z_α, τ) on the surface is given by

$$u_s(z_\alpha, \tau) = \sum_{l_1,l_2} \sum_{k} e_{gs}(z_\alpha, \tau + \mathbf{l} + \mathbf{m}_k) \ .$$ (2.24)

$1 + \mathbf{m}_k$ is a vector that gives the location of the kth atom in the unit cell and the location of the unit cell is given by 1. e_{gs} is the interaction potential between a single fluid and solid atom. We define a vector $\mathbf{t} = \tau + 1 + \mathbf{m}_k$ and write

$$g(z_\alpha) = 1/a_s \sum_k \exp(i\mathbf{g} \cdot \mathbf{m}_k) \int_A \exp(-i\mathbf{g} \cdot \tau) e_{gs}(z_\alpha, t) dt \ . \qquad (2.25)$$

The interaction potential between each solid wall atom and fluid atom is given by

$$e_{gs} = 4\varepsilon_{gs} \left[(\sigma/r_{ij})^{12} - (\sigma/r_{ij})^6 \right] , \qquad (2.26)$$

where r_{ij} = the separation distance between i^{th} fluid atom and j^{th} solid atom, The separation distance can be written as $\rho = (z_\alpha^2 + t^2)^{1/2}$. The above integral can be integrated over the orientation of τ to obtain

$$w_g(z_\alpha) = 2\pi/a_s \sum_k \exp(i\mathbf{g} \cdot \mathbf{m}_k) \int_0^\infty J_0(gt) e_{gs}(\rho) t dt, \qquad (2.27)$$

J_0 is the zeroth order Bessel Function. Now from the properties of the Bessel function,

$$\int_0^\infty J_0(gt)(1/z^2 + t^2)^{n+1} t dt = \frac{1}{n!}(g/2z)^n K_n(gz), \qquad (2.28)$$

K_n is the modified Bessel Function of the second kind. For the smooth structureless wall $\mathbf{g} = 0$, and the modified Bessel function is given by,

$$\lim_{g \to 0} \frac{1}{n!}(g/2z)^n K_n(gz) = \frac{1}{2n}z^{2n}, \ \ n > 0 \ . \qquad (2.29)$$
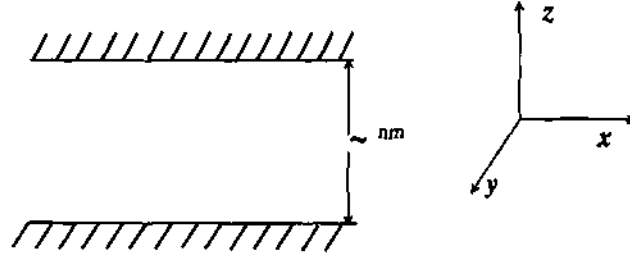
Figure 2.2: The channel is unbounded in x and y directions through the application of periodic boundary conditions and in the z direction it is bounded by the walls on both sides.

For 12-6 Lennard Jones potential, the final expression for the surface potential becomes,

$$u_s(\mathbf{r}) = 2\pi\varepsilon_{gs}q/a_s \sum (2/5(\sigma_{gs})^{12}/(z_\alpha)^{10} - (\sigma_{gs})^6/(z_\alpha)^4), \qquad (2.30)$$

where q is the total number of atoms per unit surface cell and a_s is the surface area of a unit cell.

2.5 Flow geometry

In the present study we are considering a flow system which is confined along the z direction by the walls on both sides and extended infinitely along x and y by the application of periodic boundary conditions. The geometry of the flow system is shown in Fig. 2.2. The height of the channel along the z direction is $3.78nm$ (11.1σ). In the present simulation two types of walls are considered.

(i) The smooth structureless wall, which is modelled by the 10-4 Lennard-Jones potential.

(ii) Atomic wall with atoms sitting at lattice sites.

Atomic wall is made up of atomic planes. Each atomic plane is taken as the {001} fcc planes. The wall atoms interact with the fluid atoms through the Lennard Jones 12-6 potential. Regarding the dynamics of the wall atoms, two distinct cases have been studied, firstly the wall atoms are assumed to be highly massive and therefore kept static at their respective lattice sites. In this case wall on each side is made up of two atomic layers. In the second case, the wall atoms are allowed to move about their mean positions in response to collisions sufferred with the fluid atoms. Here, 12-6 Lennard Jones interaction is considered between the wall atoms and a constant temperature is maintained at the wall by the application of an artificial thermostat. Through the interaction with the wall, the fluid attains thermal equilibrium and a constant temperature condition results in the flow system. In this case, wall on each side is made up of four atomic layers. The wall atoms in outer two layers on both sides are assumed to be highly massive and kept static during the simulation. They mimic the presence of the bulk solid. The atoms in the inner two wall-layers are interacting with the fluid atoms as well as with all other wall atoms and suffer displacements about their mean positions. The wall-wall interaction strength is taken as six times of the fluid-fluid interaction to prevent melting of the wall layers.

2.6   Constant temperature molecular dynamics

A constant temperature ensemble can be generated in various ways, *e.g.*, by the method of constraint. In this method a friction term is added to Newton's

equation of motion. The modified equation of motion is given by,

$$\dot{\mathbf{p}} = \mathbf{f} - \xi(\mathbf{r}, \mathbf{p})\mathbf{p} \ . \tag{2.31}$$

The quantity $\xi(\mathbf{rp})\mathbf{p}$ is a friction term and $\xi(\mathbf{r}, \mathbf{p})$ is called the friction coefficient, which is varied so as to keep the mean kinetic energy of the system constant. The method is implemented as follows.

1. Make an unconstrained half step,

$$\dot{\mathbf{r}}(t) = \dot{\mathbf{r}}(t - \delta t) + (1/2)\mathbf{f}(t)\delta t/m \ . \tag{2.32}$$

2. Calculate $\chi = (T/T')$ where T is the desired temperature and T' is the instantaneous temperature from these unconstrained velocities. χ is related to ξ through the following relation

$$(\chi)^{-1} = 1 + (1/2)\xi\delta t \ . \tag{2.33}$$

3. Complete the full step using

$$\dot{\mathbf{r}}(t + \delta t) = (2\chi - 1)\dot{\mathbf{r}}(t - \delta t) + (1/2)\chi \ \mathbf{f}(t)\delta t/m \ . \tag{2.34}$$

The above method is used for the temperature control in the present simulation.

2.7   Simulation Procedure

Simulations are carried out in the following sequence.

1. Initialization.

2. Melting and equilibration.

3. Imposition of flow in the equilibrated system.

4. Calculation of the desired average properties.

Initialization

The initial positions of the atoms are assigned with the constraint that the least distance between two atomic centers is 1.0, which defines the diameter of an atom. When atoms are given initial positions by random trials, then the probability of finding available space for an atomic center decays exponentially with density. Consequently with the higher density of the liquid this initialization process becomes even more difficult and takes a lot of computation time. In the present simulation the density used is 0.8. So, to make this process more efficient all the atoms are placed on an fcc lattice and then this system is melted and equilibrated to give a liquid configuration. The initial system is unbounded along the x and y directions by the application of periodic boundary conditions in these directions, while in the z direction it is bounded by the walls on both sides. The initial velocities given are gaussian random numbers of zero mean and variance $\sqrt{T}$, where T is the temperature of the system.

Melting and equilibration

The initial lattice system is allowed to melt following constant temperature molecular dynamics steps. Simple velocity rescaling is used to keep the fluid

temperature constant during melting period. Equilibration is tracked by following few order parameters with time.

Calculation of the desired average properties

In the equilibrated system required conditions are imposed, such as inclusion of the wall potential at upper and lower z position for the smooth wall case, imposing a body force on every atom in the equilibrated system to simulate the Poiseuille flow etc. After introducing these constraints and conditions in the system all the desired time averaged properties such as density profile (in the static fluid), velocity profile have been calculated over a reasonably long period of time.

2.8   Unit system

The mass and diameter of the atom is taken as the unit of mass and length. The interaction strength between the atoms is taken as the unit of energy. All the other units are derived from these three units. This reduced unit system has been used throughout the present simulation. The units of the relevant physical variables are evaluated in terms of Lennard-Jones parameters of Argon and given in the appendix.

CHAPTER 3

Density profile

3.1 Melting and equilibration of the initial lattice structure

a) Initial configuration

An ordered arrangement of atoms sitting at fcc lattice site is taken as an initial configuration as discussed in the previous chapter. This system is melted and equilibrated through constant temperature MD (molecular dynamics) steps which finally gives a disordered spatial distribution of atoms characteristics of the liquid state. The initial configuration of the atoms is shown in Fig. 3.1. This equilibrated system is the starting point of all the simulations carried out in the present study. Volume as well as lattice spacing is calculated from the initial density and total number of particles both of which are fixed parameters in this simulation. The density of the system is taken as 0.8 and the corresponding lattice spacing is 1.7099σ, and the initial temperature is set to 1.2. The initial velocity components are drawn from a random gaussian distribution of zero mean and variance $\sqrt{T}$. During the melting period the temperature of the system is kept constant by the rescaling of the velocities of individual atoms.
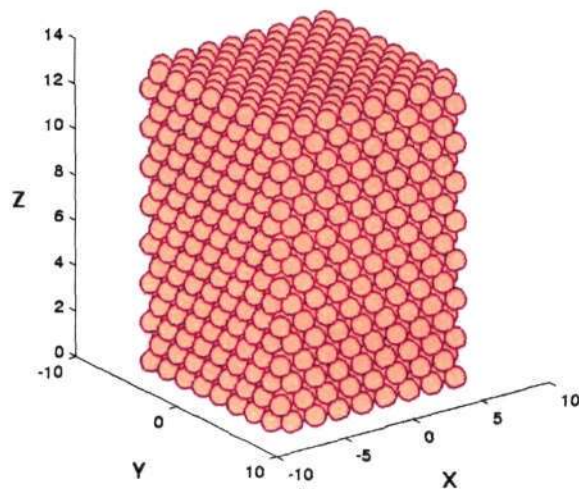
Figure 3.1: The figure shows the initial configuration of simulation system.

b)   Tracking of equilibration

To keep track of melting and equilibration a number of properties related to the configuration of the system are recorded at each time step during this period and plotted as a function of time. The step size in the simulation is taken as 0.004.

c)   Potential energy of the system

As seen from Fig. 3.2, the kinetic energy remains constant and the total energy follows the potential energy profile. The initial potential energy of the system has a large negative value representing the initial close packed ordered system. Within the first 200 time steps the potential energy rises smoothly,
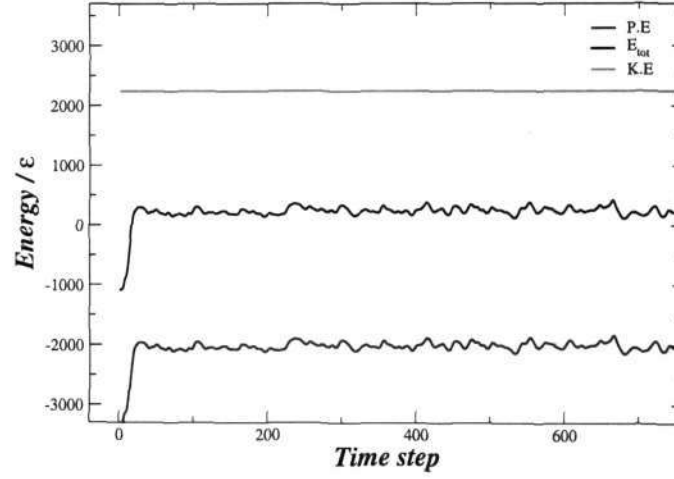
Figure 3.2: Variation of the total energy, kinetic energy and potential energy with time is shown. The kinetic energy remains constant, whereas the total energy and the potential energy rise with time. The well depth of the potential ε is taken as the unit of energy here.

as well. It implies that the system has reached its equilibrium configuration.

d)   Translational order parameter

The translational order parameter is defined as

$$P_{tr} = \frac{1}{n} \sum_i \cos \mathbf{k}.\mathbf{r}_i$$

where n is total number of atoms in the system, $\mathbf{r}_i$ is the position vector of the center of mass of the ith atom, and $\mathbf{k}$ is the reciprocal lattice vector of the initial fcc lattice. The translational order parameter should be of the order of unity in a perfect fcc lattice system, and fluctuates with an amplitude of $O(n^{-1/2})$ around zero due to the random variation of the phase factor $\mathbf{k}.\mathbf{r}_i$ in a disordered system. From Fig. 3.4, the variation of the translational
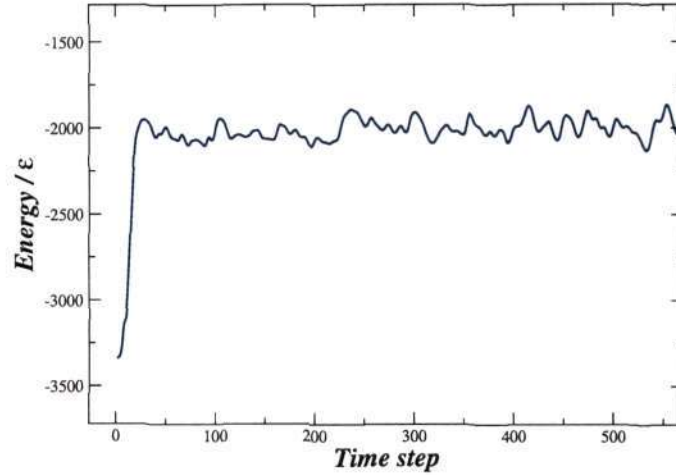
Figure 3.3: The variation of potential energy with time (magnification of portion of Fig. 3.2).

order parameter shows the system has reached a disordered configuration approximately after about 500 time steps, beginning from an ordered state.

e)   Structure factor

The particle density ρ in a lattice is periodic in space with the periodicity of the lattice. Then at any point $\mathbf{r}$ inside the lattice the local density can be written as

$$\rho(\mathbf{r}) = \sum_i \delta(\mathbf{r} - \mathbf{r}_i)$$

where r_i is the position of the ith site. The Fourier amplitude of this density distribution is given by,

$$\rho_k = \int \exp(-i\mathbf{k}.\mathbf{r})\rho(\mathbf{r}) = \sum_k \exp(-i\mathbf{k}.\mathbf{r}_j).$$
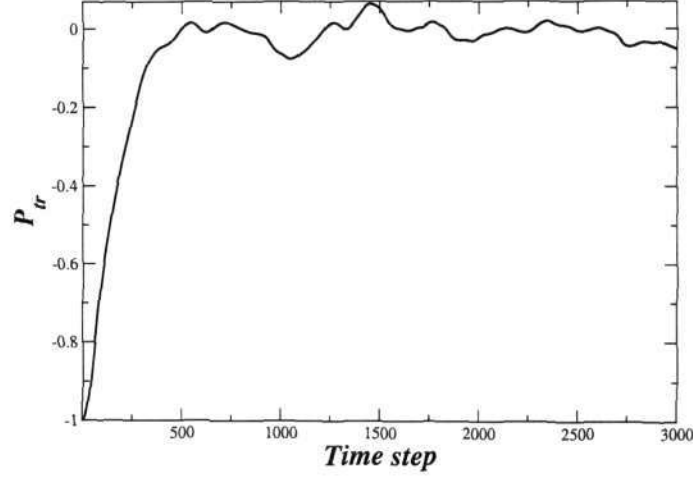
Figure 3.4: Variation of the translational order parameter as a function of time. Starting from an absolute value of 1, translational order parameter drops down and reaches near zero, indicating a transition from lattice state to disordered state.

The structure factor (Hansen & Mcdonald (1986)) is defined as

$$s(k) = \frac{1}{n} \langle \rho_k^* \rho_k \rangle = \frac{1}{n} \sum_j \sum_{l \neq j} \exp(-i\mathbf{k}(\mathbf{r}_j - \mathbf{r}_l)).$$

n is the total number of atoms present in the simulation box and the averaging can be either time averaging or ensemble averaging. Here, the instantaneous structure factor for a fixed k value is recorded (k is the reciprocal lattice vector for the initial lattice) and plotted as a function of time. In Fig. 3.5 the structure factor goes down to near zero starting from an initial finite value within the first few time steps and then fluctuates around a small value near zero in subsequent time, indicating a transition from an lattice to an disordered state and equilibration of the latter.
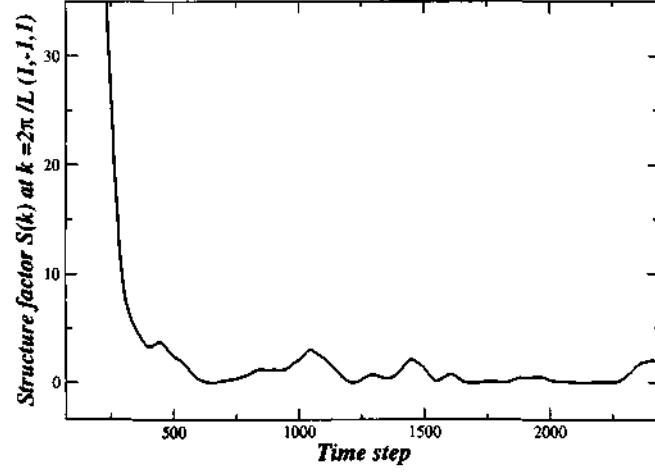
Figure 3.5: The structure factor as a function of time is shown. The value
of k is taken as $(2\pi/L)(1, -1, 1)$ where L is the boxlength, at this value of k
the structure factor of the fcc lattice has a high value. This value falls down
to near zero as the liquid state is attained.

f)   Pair distribution function

The pair distribution function of a system provides information about the
structure of a system. This quantity can be measured experimentally from
thermal neutron and X-ray scattering experiment on simple fluids, and light
scattering experiments on colloidal suspensions, which can be compared with
the numerical result. In a system of N particles of volume V and tempera-
ture T, the probability that the molecule 1 is between r_1 and $r_1 + dr_1$, 2 is
between dr_2 and $r_2 + dr_2$ and so on up to the molecule n, irrespective of the
configuration of the remaining $N - n$ molecules is given by,

$$p^n(\mathbf{r}_1, ... \mathbf{r}_n) = \int .... \int \exp(-\beta U_n) d\mathbf{r}^{n+1} ... d\mathbf{r}_N. \tag{3.1}$$

Now the probability that any one molecule out of the N molecules is between $\mathbf{r}_1$ and $\mathbf{r}_1 + d\mathbf{r}_1$, is given by

$$\rho^n(\mathbf{r}_1, ...\mathbf{r}_n) = \frac{N!}{(N-n)!} \ p^n(\mathbf{r}_1, ...\mathbf{r}_n). \tag{3.2}$$

A correlation function is defined by the following relation,

$$\rho^{(n)}(\mathbf{r}_1, \mathbf{r}_2, ..\mathbf{r}_n) = \rho^n g^n(\mathbf{r}_1, \mathbf{r}_2, ...\mathbf{r}_n),$$

g^n is called the correlation function since if the molecules were independent of each other, $\rho^{(n)}$ would simply be ρ^n. The factor g^n includes the effect of the correlation between the molecules. The two particle correlation function is given by,

$$\rho(\mathbf{r}_1, \mathbf{r}_2) = \rho^2 g^2(\mathbf{r}_1, \mathbf{r}_2).$$

In a liquid of spherically symmetric interactions, $g^2(\mathbf{r}_1, \mathbf{r}_2)$ depends only upon the relative distance between the molecules 1 and 2, i.e upon r_{12}. So we can write,

$$g^2(\mathbf{r}_1, \mathbf{r}_2) = g(r),$$

where r is the separation between the two molecules and $g(r)$ is the probability of finding two atoms separated by a distance r. $g(r)$ is called the pair distribution function. Alternatively a normalized pair distribution function can be defined as,

$$g(r) = n(r)/n^i(r).$$

$n(r)$ is the average particle density at a distance r from a central atom and $n^i(r)$ is the same for an ideal gas. At large r, $n(r) \rightarrow n^i(r)$ and $g(r) \rightarrow 1$ This is a working definition used to calculate $g(r)$ in a simulation. Now for

an ideal gas, there is no interaction between the atoms, so atoms are equally probable at all separations from a particular atom, implying ρ is uniform everywhere. So the probability of getting one atom at a distance r from the central atom is proportional to the fraction of the shell volume between r and $r + dr$ of the total volume V. This fraction is

$$4\pi r^2 dr/V.$$

So the number of atoms lying in this shell is given by

$$n^i(r) = 4\pi r^2 dr(N/V),$$

where N is the total number of particles of the system. Hence the pair distribution function is given by,

$$g(r) = \frac{n(r)}{4\pi r^2 \rho dr}.$$

In the present simulation $g(r)$ is first calculated for the initial lattice configuration before the starting of the run. The Fig. 3.6 shows the initial $g(r)$. This plot contains sharply rising peaks at some discrete points on the horizontal axis and zero in-between. This well spaced discrete distribution is expected for a lattice structure. In the fcc structure, peaks should occur at $a/\sqrt{2}$, a, $\sqrt{\frac{3}{2}}a$, $\sqrt{2}a$, $\sqrt{5}a/2$, $\sqrt{3}a$. Here the lattice constant is 1.709σ, the peaks in the above figure are at 1.208, 1.7099, 2.101, 2.418, 2.705, 2.95 etc. which conform to the expected distances. In the present study, the total simulation run period is divided into successive blocks and over each block of time the pair distribution function is averaged separately to observe the change in structure of the system undergoing melting. Smaller blocks are
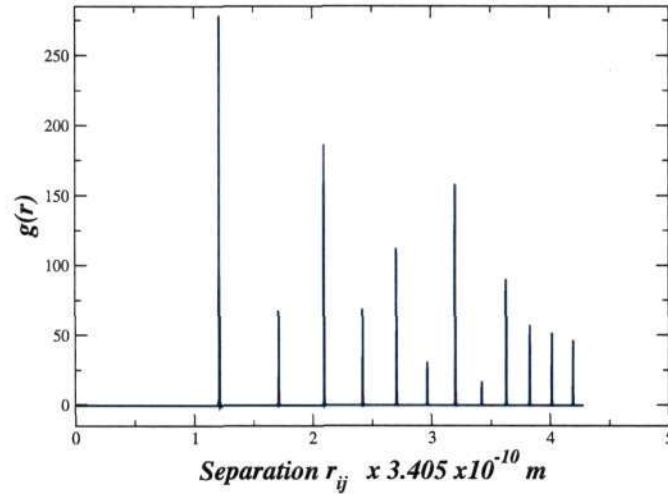
Figure 3.6: Pair distribution function of initial lattice configuration, shows a well spaced discrete distribution representative of the lattice state, time step used is 0.004.

taken during the initial transition period. The pair distribution functions obtained in successive averages are shown in Fig. 3.7-3.13.

These figures carry some signature of both solid and liquid phases and clearly show the gradual change of the structure during a transition from an ordered to a disordered state. We note, firstly, that the pair distribution function is always almost zero at separation distances less than unity which indicates the fact that the atoms do not penetrate each other below that distance. This is due to the highly repulsive nature of the Lennard-Jones potential at short range. The width about the discrete lines in Fig. 3.7 shows that the atoms have started fluctuating about their lattice sites. Fig. 3.8 shows widths are broadened, which implies large displacements of the atoms about their mean positions, which is the onset of the disorder. The next two figures show the periodicity of the initial lattice is dying down and a new "order", characteristic of a liquid state is establishing gradually. Fig. 3.13
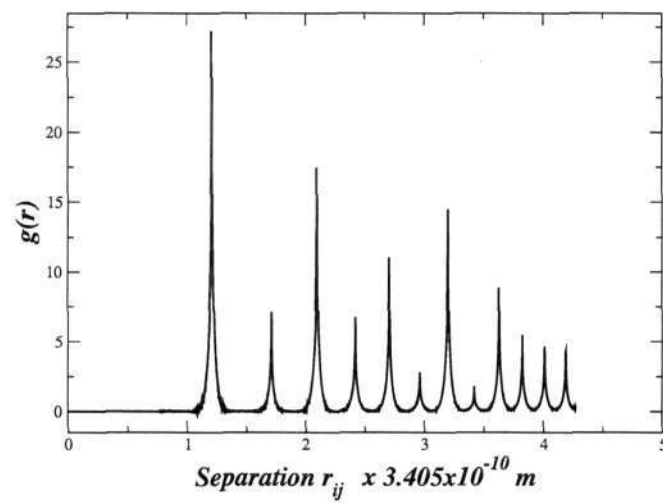
Figure 3.7: Pair distribution function averaged over 0-50 steps. The finite width around discrete lines arises due to the thermal agitation of the atoms around their mean.
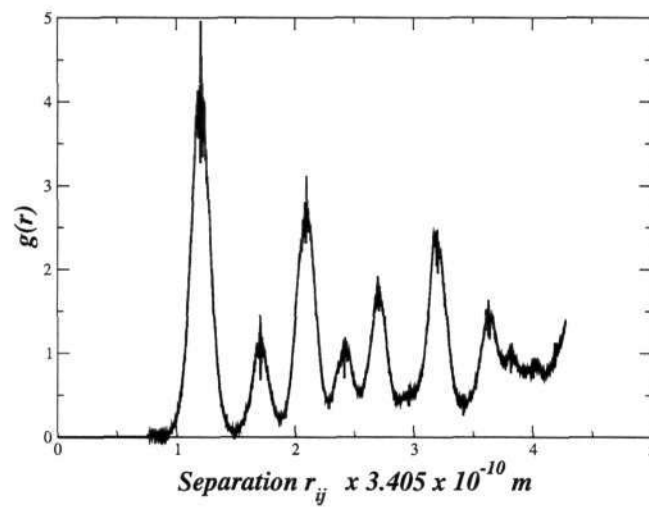
Figure 3.8: Pair distribution function averaged over 50-100 steps, shows the widths are broadening around the peaks.
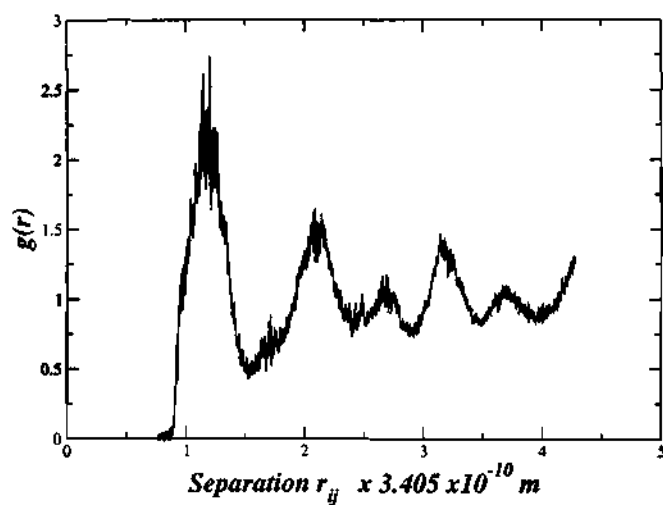
Figure 3.9: Pair distribution function averaged over 100-200 steps.
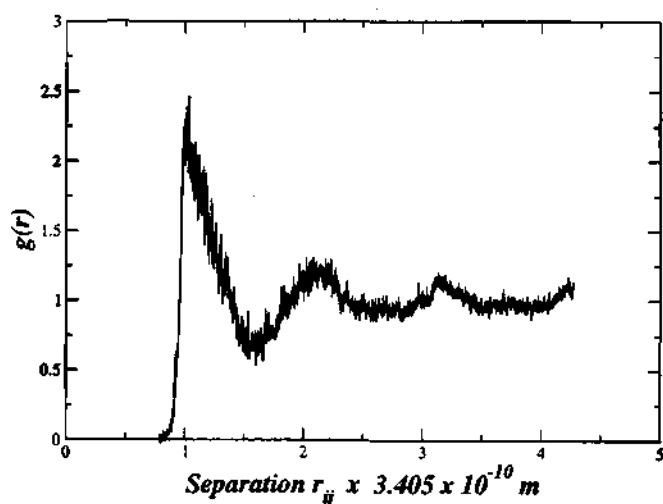
Figure 3.10: Pair distribution function averaged on 200-300 steps, a new order is establishing itself.
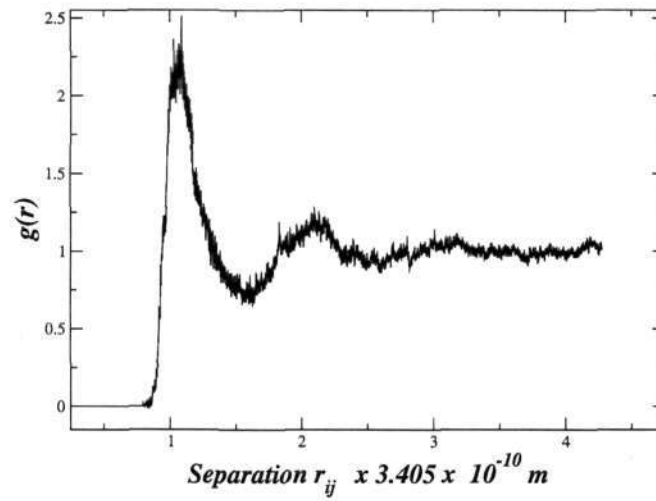
Figure 3.11: Pair distribution function averaged over 300-500 steps.
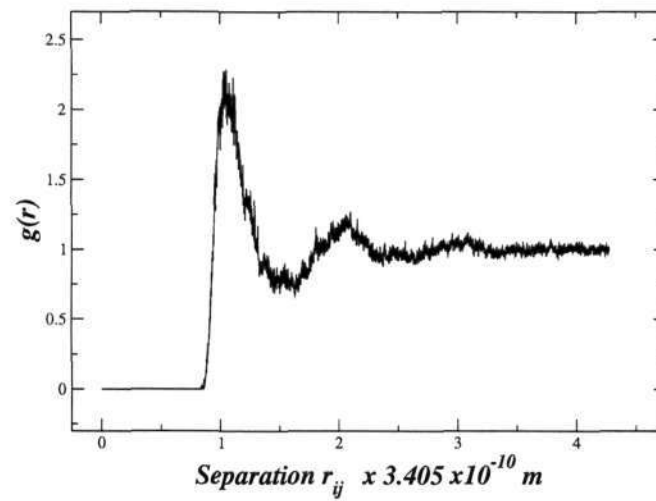
Figure 3.12: Pair distribution function averaged over 500-700 steps.
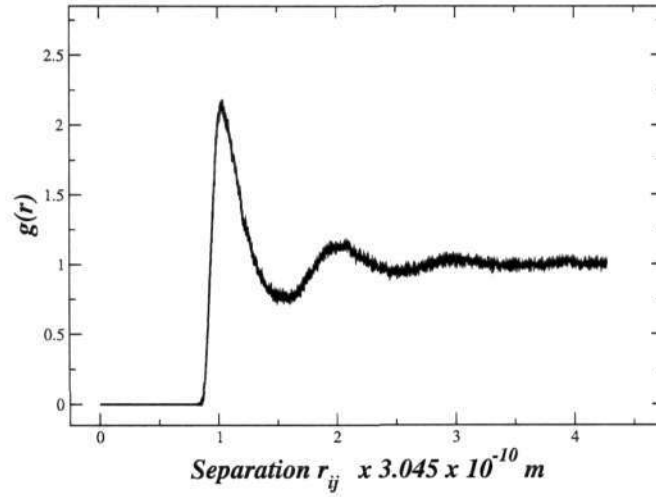
Figure 3.13: Pair distribution function averaged over 700-2000 time steps. A short range order typical of liquids is seen.

is obtained by averaging over a long period of time giving the typical pair distribution function of a liquid. Pair distribution function contains peaks at $\sigma, 2\sigma, 3\sigma$, which show that a short range order exists in liquids and it converges (maximum separation considered here is half the boxlength) to unity at large separations.

3.2   Density profile

The density variation across a nano-channel with two different kinds of wall-structured and unstructured, is investigated. The system under study (as mentioned in chapter two) is a channel confined by two walls along z direction and infinitely extended along x and y. To obtain the density profile across the channel, the channel is divided into a number of bins along the z direction and then the number of atoms per bin is calculated at each time step. This quantity is time averaged to give a averaged number density per
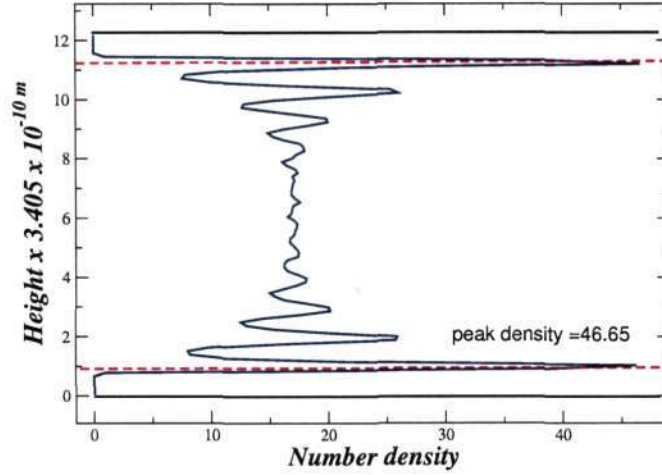
Figure 3.14: The above figure shows the density profile across the channel with smooth walls on the both sides. The upper and lower wall are at $z = 12.254$ and $z = 0.0$ respectively. The upper and lower peaks in the density profile appear at a z value of 11.22 and 1.04 respectively. The peak density observed is 46.65. The dashed line shows the position of minimum of the 10-4 potential.

bin. The density profile shows a sharp well localized main peak and a few modulations near each wall, whereas in the middle of the channel there are only small deviations about a constant value that corresponds to the bulk number density. A typical profile obtained with the smooth wall (Lennard Jones 10-4 potential) is shown in Fig. 3.14. The height of the channel is $4.17nm$. The upper wall position is at $z = 12.254$ whereas the lower wall is placed at $z = 0.0$.

The density profile with an atomic wall (001 fcc lattice) on both sides is shown in Fig. 3.15. In this simulation a system with 1536 fluid atoms with 256 wall atoms on each side is considered. Each wall is composed of two atomic layers, each of which is a 001 fcc lattice plane made up of 128 atoms. The lower and upper wall positions are at $z = 0.86$ and $z = 11.96$ respectively. Wall atoms are assumed to have a very high mass and hence kept static during the

simulation. The wall-fluid and fluid-fluid interaction is taken to be identical. The state point used is $\rho = 0.8, T = 1.2$. Fig. 3.14-3.15 show the density
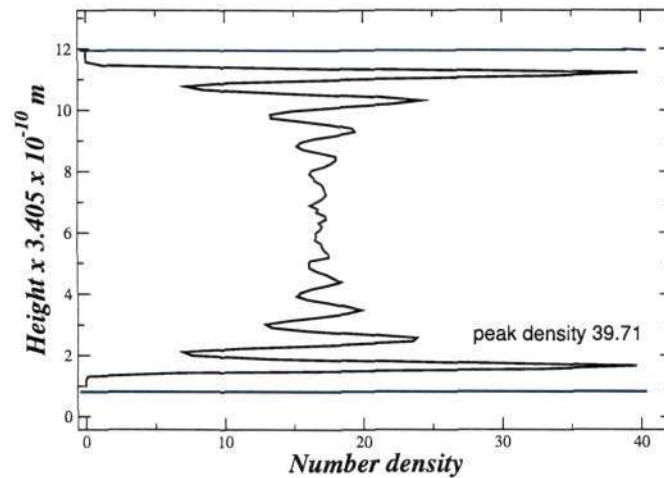
Figure 3.15: Density profile with atomic wall (static), The upper and lower wall are at $z = 11.96$ and $z = 0.86$ respectively. The upper and lower peak appear at $z = 11.21$ and at $z = 1.63$ and peak density is 39.71.

profiles with smooth and atomic walls respectively. Both are qualitatively same. However the distance of the first peak from the wall and the amplitude of the first peak differs in the two cases. For the smooth wall the first peak forms at a distance 1.03 away from the wall whereas for the atomic wall it is at a distance 0.77 away from the wall. The amplitude of the first peak is 46.65 and 39.46 for the smooth and atomic walls respectively. The presence of the wall creates a potential minima causing the observed near-wall peaks in density profile. The next few oscillations in the density profile arise from the short range order $(g(r))$ that exists in liquid.

The minimum of the smooth wall potential $(10 - 4$ Lennard-Jones$)$ is at 1.0, consistent with the first peak distance (1.03) from the wall. The potential surface for the smooth wall case is a continuous one, but for the
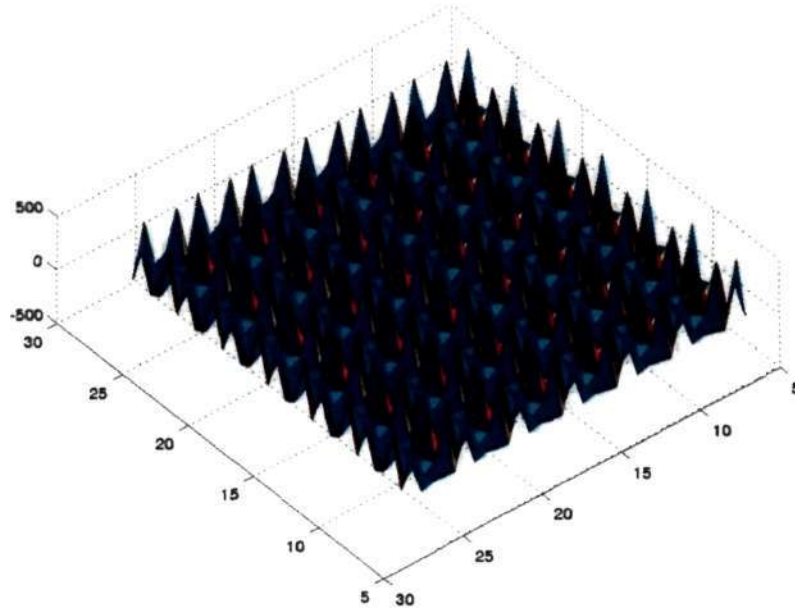
Figure 3.16: Corrugated surface potential at a height of 0.86 from the lattice planes.

atomic wall potential surface is corrugated with local minima and maxima distributed periodically. Figure 3.16 shows the top view of such a potential surface. A 2D mesh is taken over the lattice planes and the potential due to it is calculated at every point. Fluid atoms are found preferentially at these minima which explains the peak height (0.77) from the wall. A comparison of these potential surfaces again explains the higher number density of fluid atoms in case of smooth wall over the atomic wall with the same wall-fluid interaction strength (e_{wf}=1.0). To verify the $x - y$ position of fluid atoms with respect to the wall atoms a snapshot of of the $x - y$ postion of near wall fluid atoms is taken and projected over the $x - y$ position of wall atoms. It shows fluid atoms are preferentially sitting at the local minima and the corrugated potential induces a parallel order ($x - y$) in the fluid layer nearest
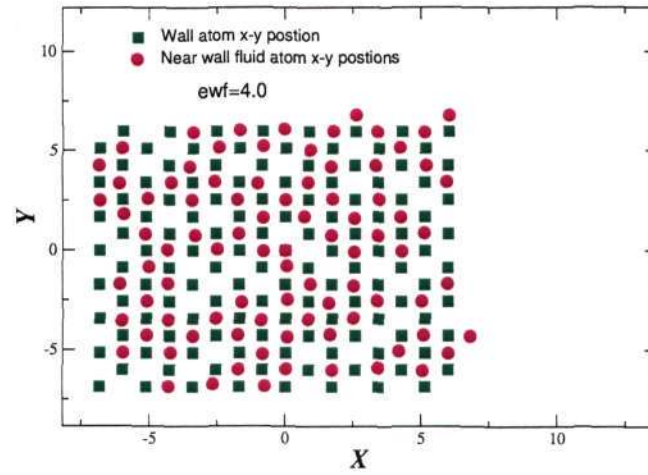
Figure 3.17: Projection of the $x-y$ position of near wall fluid atom (magenta) over the $x-y$ position of the wall (green) atoms, distance of the fluid layer from the wall is 0.77, binwidth= 0.111.

to the wall.

The density profile for the case of a wall-fluid interaction strength twice that of the fluid-fluid strength is shown in the Figure 3.18. The magnitude of the near-wall peak increases with a higher strength. Due to the increase of the strength of wall fluid interaction local minimum on the potential surface becomes deeper and the probability of a near-wall fluid atom of being trapped in these wells becomes higher which results increased peaks in the density profile.
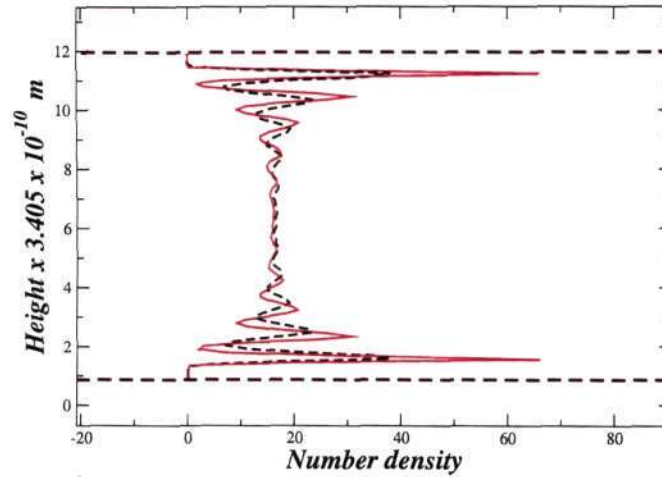
Figure 3.18: Density profile with two different wall fluid interaction strength (e_{wf}) is shown. The red solid line corresponds to $e_{wf} = 2.0$ whereas the the dashed line is for $e_{wf} = 1.0$. The number of bins used are 100.

3.3 Comparison with the results in the literature

The present code is validated with the simulation results obtained by Koplik *et al.* (1988). They considered an identical flow system with 1536 fluid atoms and static atomic walls on both the sides, the density and the temperature used in their simulation were 0.8 and 1.2 respectively. The present simulation is carried out with the same parameters and the scaled (density per unit length) density profile is compared with with their profile (scaled similarly). Figure 3.19 shows the comparison, the present result matches very well with their profile.
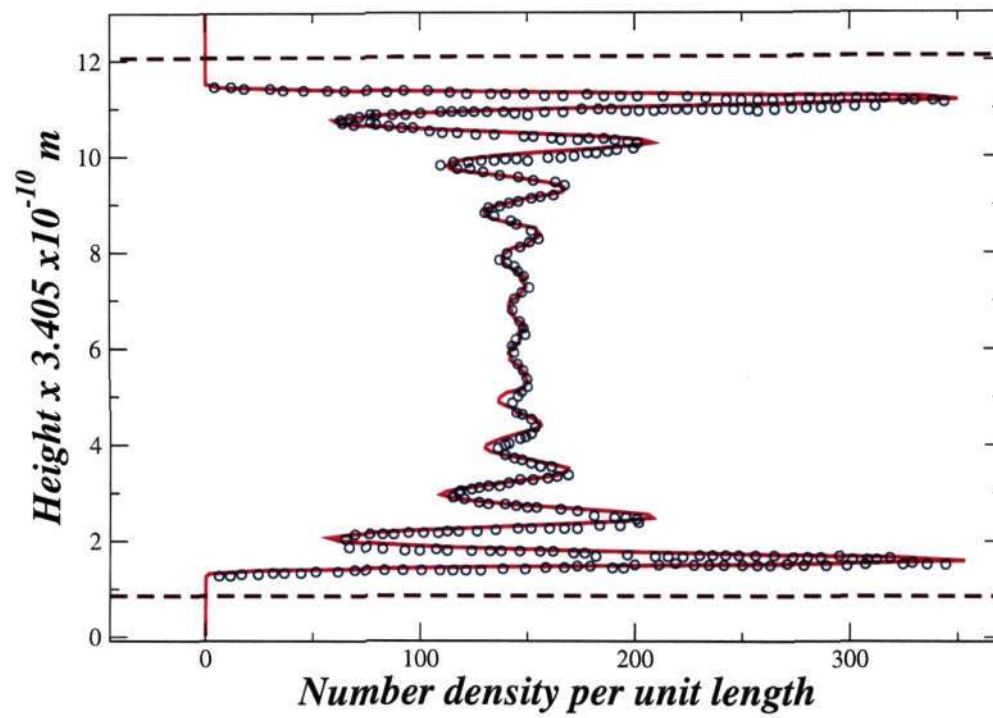
Figure 3.19: Validation of the present code, the solid red line is the present result and and blue dots are the data from Koplik et al. The number of atoms used are 1536. The density and temperature are 0.8 and 1.2 respectively.

CHAPTER 4

Simulation of plane Poiseuille flow with static walls

4.1 Simulation of plane Poiseuille flow

Poiseuille flow is simulated in a channel with atomic walls on both sides. Wall atoms are assumed to have very high mass and therefore remain static during the simulation. Each wall consists of 256 atoms and the number of
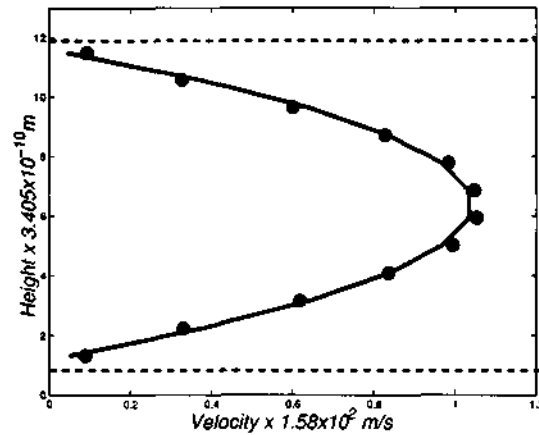
Figure 4.1: The figure shows the simulated velocity profile (black circles) in the channel at a body force 0.2. The solid line is a parabolic fit to the simulated profile. The channel height is 3.78 nm or 11.1σ.

fluid atoms used is 1536. A constant body force along the x direction is imposed on each of the fluid atoms.
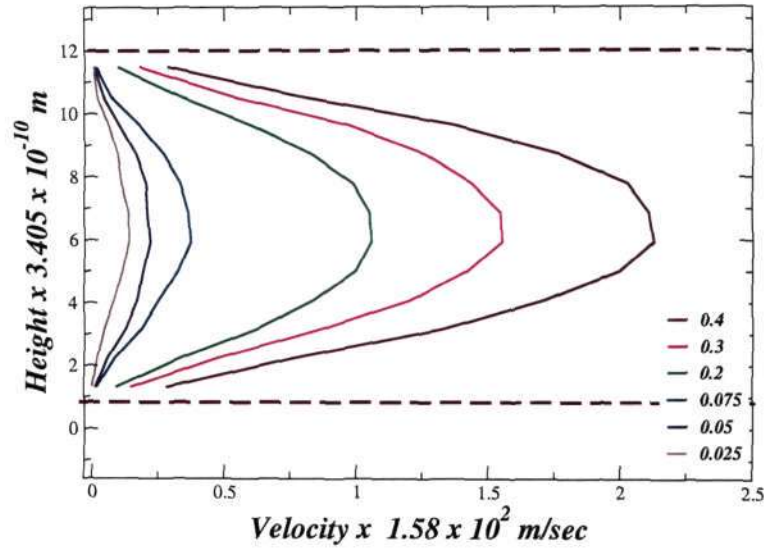
Figure 4.2: The figure shows velocity profiles at different body forces.

The velocity profile is computed by binning the particles along the z direction and finding the average velocity in each bin, 12 bins are considered in the present simulation. A velocity profile simulated for a body force of 0.2 and a parabolic fit to it is shown in Fig. 4.1. The velocity profile at different body forces is shown in Fig. 4.2 which shows the velocity at the centerline increases with the body force. The centerline velocities are plotted at different body forces separately in (Fig. 4.3). It is seen that the centerline velocity scales with the body force. A set of velocity profiles has been obtained through block averaging over intervals of time of 50000 time steps each. Fig. 4.4 shows data points for three such block averages for a body force 0.1 and the solid line is a fit from Navier Stokes equation. It is seen that the data sets are well defined and distributed around one mean profile which indicates flow has reached a steady state.

Figure 4.5 shows velocity profiles with a higher wall fluid interaction ($e_{wf} =$
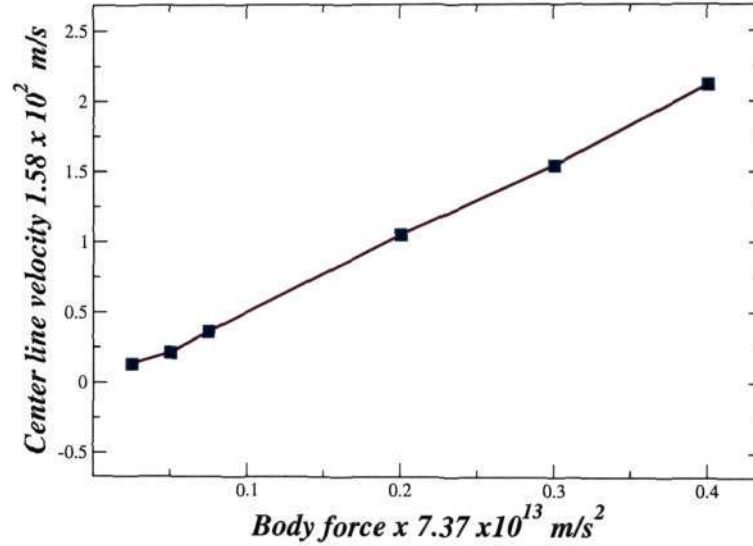
Figure 4.3: The figure shows centerline velocity as a function of the body force. It shows centerline velocity scales with the body force as expected from continuum theory.

2.5). Higher wall-fluid interaction increases the sticking of fluid atoms to the wall, the first fluid layer becomes completely locked to the wall and forms an effective wall while the second fluid layer slips over the first. This locking is manifested in the "jump" that appears in the velocity profile near the wall.

4.2 Derivation of Poiseuille flow profile from Navier-Stokes equation

The Navier Stokes equation is given by,

$$\rho Dv/Dt = g - \nabla p + \mu \nabla^2 v, \qquad (4.1)$$
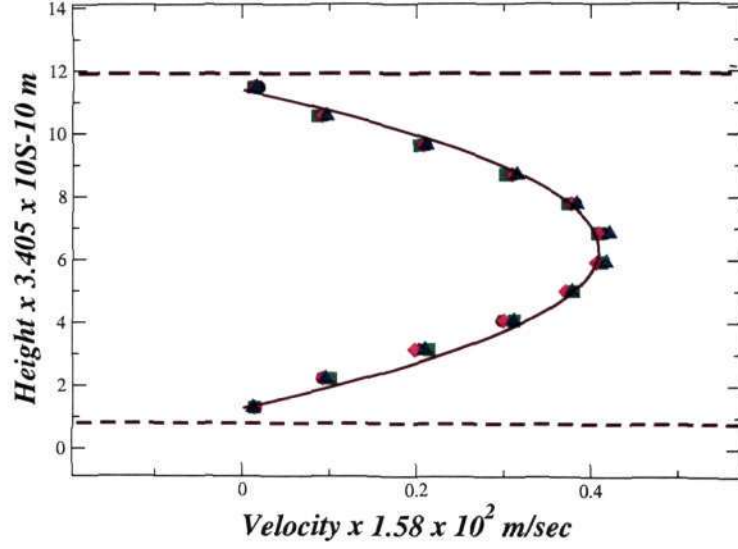
Figure 4.4: The figure shows velocity profiles averaged over sucessive intervals of time for a body force of 0.1. Each interval consists of 50000 time steps. The solid line shows a fit from Navier Stokes equation with lower and upper wall positions respectively at $z_1 = 1.28$ and $z_2 = 11.39$. The dashed line shows the wall positions $(0.86, 11.96)$.

where g is the body force acting in the system. For a steady laminar plane Poiseuille flow $Dv/Dt = 0$ and in the absence of a pressure gradient the above equation becomes

$$\mu \frac{d^2v}{dz^2} = -\rho g. \tag{4.2}$$

Integration of the above equation gives,

$$\mu \frac{dv}{dz} = -\rho g z + C_1. \tag{4.3}$$

The velocity profile is symmetric about the center line, so at

$$z_m = (z_1 + z_2)/2, \ \frac{dv}{dz} = 0, \tag{4.4}$$
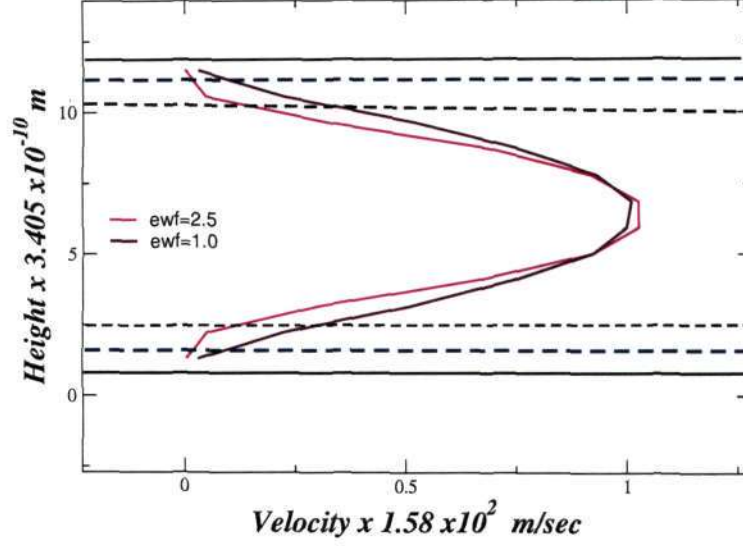
Figure 4.5: Velocity profiles at wall-fluid interaction $e_{wf} = 2.5$ and 1.0. The solid lines show the position of the actual atomic walls, blue and black dashed line show the position of the first and second peak in density profile respectively.

which gives,

$$C_1 = \rho g(z_1 + z_2)/2\mu. \tag{4.5}$$

Integrating again we get,

$$v(z) = -\rho g z^2/2\mu + \rho g z(z_1 + z_2)/2\mu + C_2. \tag{4.6}$$

Now from the no-slip condition at the wall, i.e at $z = z_1$, $v = 0$, we get,

$$C_2 = -\rho g z_1 z_2/2\mu. \tag{4.7}$$

The final expression for velocity is given by

$$v(z) = (\rho g/2\mu)(z - z_1)(z_2 - z). \tag{4.8}$$

Where z_1 = effective lower wall position,

and z_2 = effective upper wall position.

4.3   Comparison with results in the literature
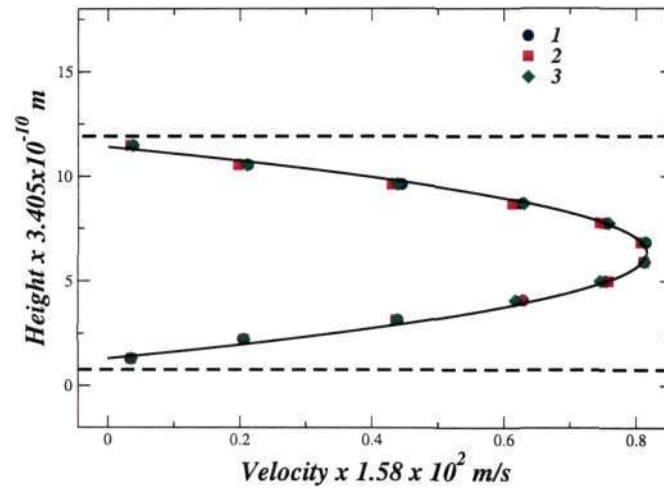
Figure 4.6: The velocity profile at a body force of 0.2 is shown. The numbers in inset indicates successive averages and each data set is averaged over 50000 steps. The dashed lines are the wall positions $(0.86, 11.96)$ and the solid line shows the fit from the Navier Stokes equation with effective wall positions $z_1 = 1.29$ and $z_2 = 11.41$.

The simulated profiles for different body forces are fitted with the profiles obtained from Navier-Stokes equation and for each one the value of viscosity is estimated. The set of viscosity values obtained in present simulations fall within the range estimated by Koplik & Banavar (1989). The table 4.1 shows both sets of viscosity values.

The effective wall positions (z_1 and z_2, see Eq. 4.8) is found to lie within the range 11.35 ± 0.15 and 1.38 ± 0.13 for all values of body forces. The table 4.2 shows upper and lower wall positions at different body forces. No

Body force $(g\tau^2/\sigma)$ $(7.39 \times 10^{13} m/sec^2)$	Viscosity (Koplik & Banavar (1988)) $(\mu\sigma\tau/m)$ $(0.9076 \times 10^{-4} kg/msec)$	Viscosity (present study) $(\mu\sigma\tau/m)$ $(0.9076 \times 10^{-4} kg/msec)$
0.025	1.85±0.5	1.78
0.05	2.05±0.5	2.3
0.075	1.98±0.5	1.99
0.1	1.85±0.25	1.98
0.2	1.80±0.15	1.85
0.4	1.80±0.15	1.82

Table 4.1: Viscosity values at different body forces from present simulation and from Koplik & Banavar (1988) are compared.

systematic variation of the wall positions is observed with the body forces.

Further analysis has been done to find the velocity of fluid layers locked to the wall. The channel is divided into 24 bins to provide a higher resolution. Figure 4.7 shows veloctiy profile for a wall-fluid interaction $e_{wf} = 2.5$ with 24 bins at a body force of 0.1. It is observed that the veloctiy of the first and second locked layer (corresponding to the first and second peak in the density profile) is 0.0002 and 0.0240 which is respectively 0.02% and 5% of the velocity at center line. So, the first two near-wall fluid layers are almost static.

Body force	Lower wall position	Upper wall position
0.025	1.51	11.32
0.05	1.44	11.24
0.075	1.49	11.22
0.10	1.85	11.32
0.20	1.80	11.40
0.30	1.37	11.40
0.40	1.22	11.54

Table 4.2: This table contains effective wall positions z_1 and z_2 at different body forces.
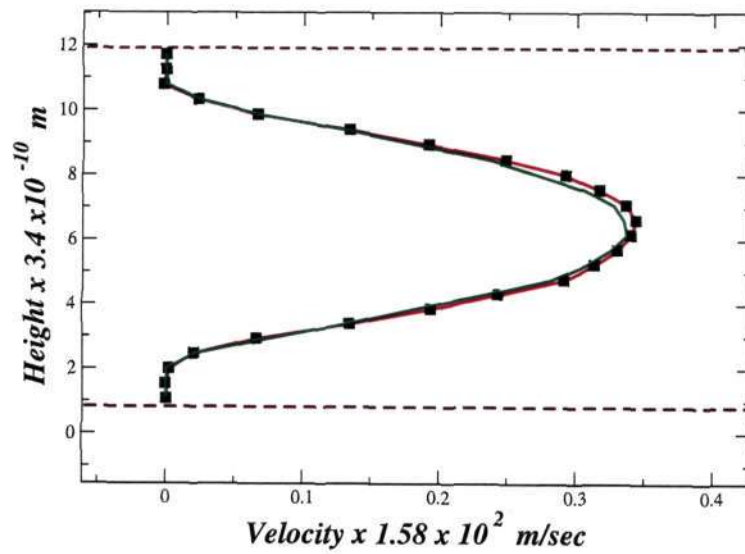
Figure 4.7: Velocity profile at the body force=0.1 with 24 bins for a wall-fluid interaction, $e_{wf} = 2.5$. The dashed lines are the wall positions $(0.86, 11.96)$.

CHAPTER 5

Simulation with walls at finite temperature

5.1   Thermalization

The body force imposed in a flow system generates thermal energy and conse-
quently the fluid temperature rises if a dissipation mechanism is not present.
Figure 5.1 shows the fluid temperature for a body force 0.02 with static wall.
Most molecular dynamics simulations of microscale flows use some artificial
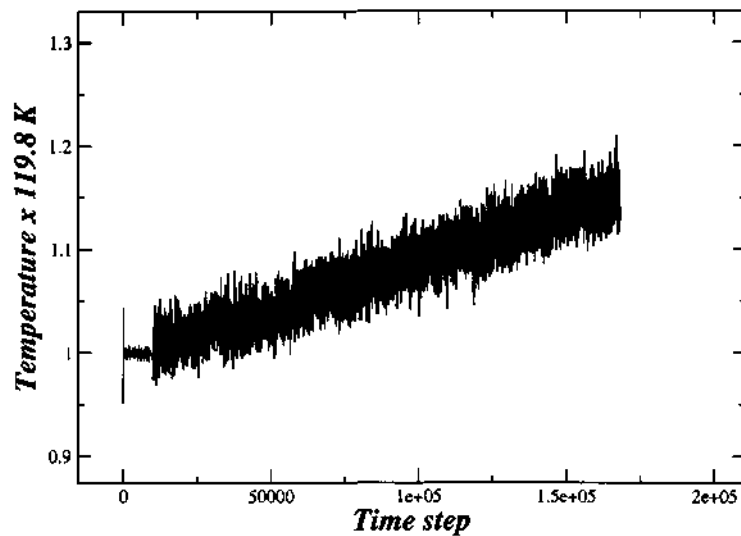
Figure 5.1: The figure shows the fluid temperature as a function of time at
a body force of 0.02. The present simulation is performed with static wall.
Initially artificial thermostat is applied to the system which gives rise to the
initial steady part of the temperature profile and after about 10000 time
steps as the thermostat is switched off, the fluid temperature starts rising as
seen from the above figure.

45

thermostat to maintain a constant fluid temperature. In the present study thermalization is achieved through realistic interaction between fluid and wall. The mass of the wall atom is taken to be fifty times that of the fluid atoms, and they are allowed to move about their mean positions in response to the collision with a fluid atom. The wall temperature is kept fixed at 1.0 by applying an artificial thermostat to the wall atoms. When the dissipation at the wall at each time step balances the generation of heat produced by the body force in the flow system then the fluid is in thermal equilibrium with the wall and a constant temperature condition results. Fig. 5.2 shows the temperature profile for a thermally equilibrated flow system. The dissipation rate depends on the collision rate and energy dissipated at each collision. Now, multiparticle collisions occurring in the middle of the channel take part in the generation process whereas only fluid atoms which are near the wall surface take part in the dissipation process. So, for a given channel width beyond a threshold acceleration, the rate of generation of thermal energy becomes too high to be completely dissipated at the walls. In the present simulation runs are made for different body forces for a fixed channel height and the threshold acceleration is found from mean temperature-acceleration curve. Figure 5.3 shows average fluid temperature as a function of acceleration. Two observations can be made regarding thermal equilibration in the present case. First, up to a body force of about 0.02 the fluid is in thermal equilibrium with the wall. Beyond this value of the body force thermal equilibration between fluid and wall is lost and but the temperature profile shows a steady state distribution and the average fluid temperature settles down at a higher value. Figures 5.4, 5.5 shows these steady state profiles. The average binwise temperature profiles across the channel are computed for the flow system under both isothermal and non-isothermal conditions. For the
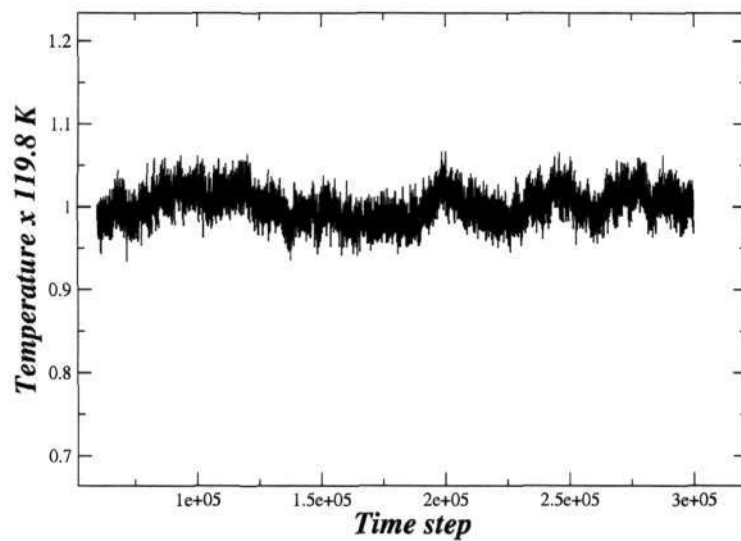
Figure 5.2: The fluid temperature as a function of time steps in a channel of
height of 3.78nm and at a body force of 0.02 is shown. The wall temperature
is kept fixed at 1.0. Thermal equilibrium exists between fluid and wall and
the mean fluid temperature settles down at 1.0.
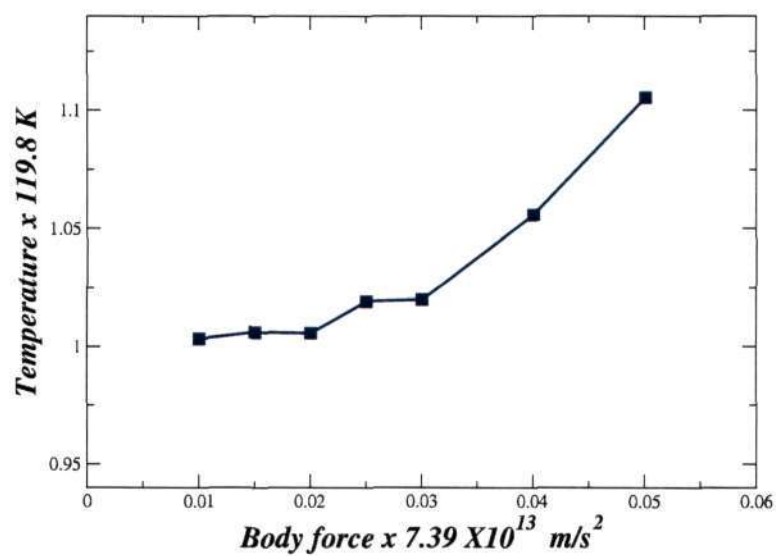
Figure 5.3: Mean fluid temperature as a function of body force is plotted. It
is seen that there exists a threshold acceleration, which is 0.02, beyond this
critical value thermal equilibration between wall and fluid is lost.
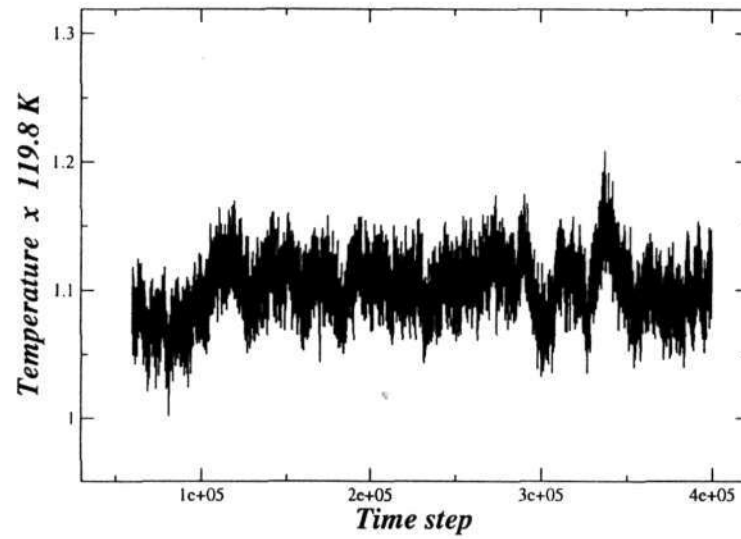
Figure 5.4: The fluid temperature as a function of time steps at a body force 0f 0.05 is shown. The thermal equilibrium between wall and fluid is lost and the mean fluid temperature settles down at a higher value of about 1.1.
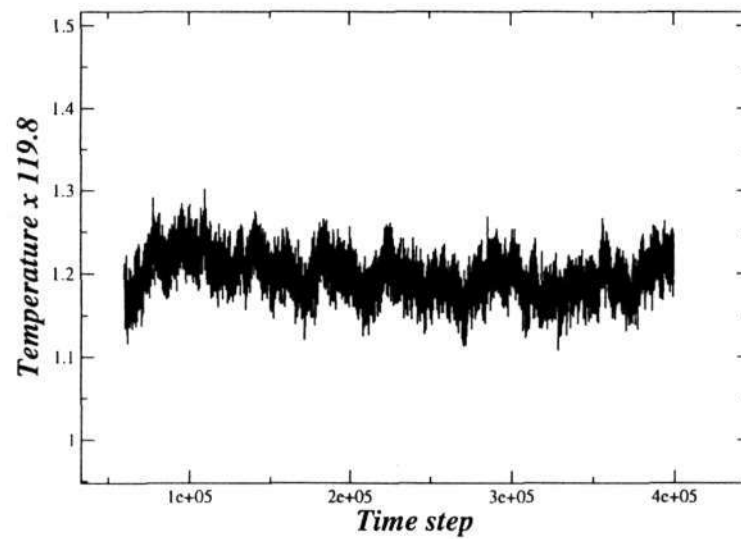
Figure 5.5: The fluid temperature as a function of time at a body force of 0.07. In this case fluid temperature settles down at value about 1.2.
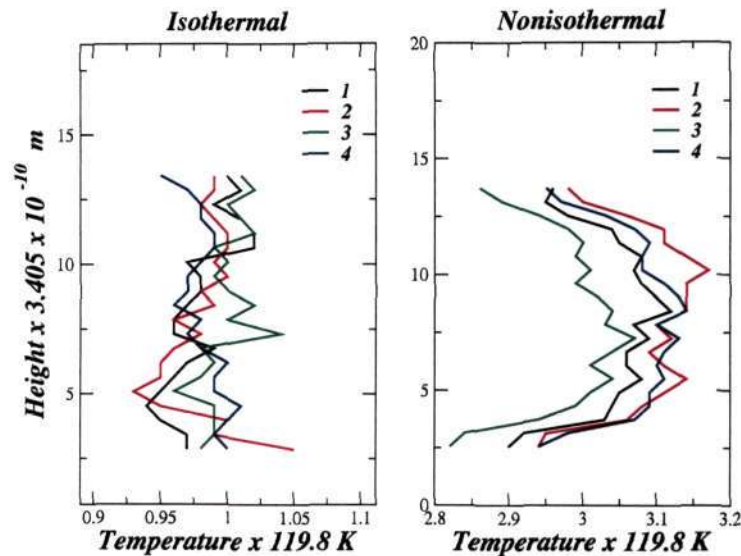
Figure 5.6: The average binwise temperature profile is shown. Each temperature profile is averaged over 25000 steps. The left figure corresponds to the isothermal case (thermal equilibration between wall and fluid exists) and obtained at a body force of 0.02. All the four temperature profiles in this case fluctuate about 1.0 (wall temperature). But at a higher body force (0.2) the temperature profile becomes a function of z as seen from the second figure which corresponds to the non-isothermal case.

isothermal case (where the fluid is in thermal equilibrium with the wall) the temperature profiles fluctuates around the equilibrium value whereas for the non-isothermal case the profiles become a function of z, Figure 5.6 shows both the cases. In the simulation described in this section, wall atoms are allowed to move about their mean position. To check the structural order of the lattice walls as simulation proceeds, translational order parameter for the first two atomic layers on both sides have been calculated. The variation of the translational order parameter with time step for the upper and lower wall are shown in Fig. 5.7 and Fig. 5.8 respectively. From a magnitude of 1.0 which represents a perfect crystal translational order parameter drops down to a lower value within the initial few time steps and then stabilizes
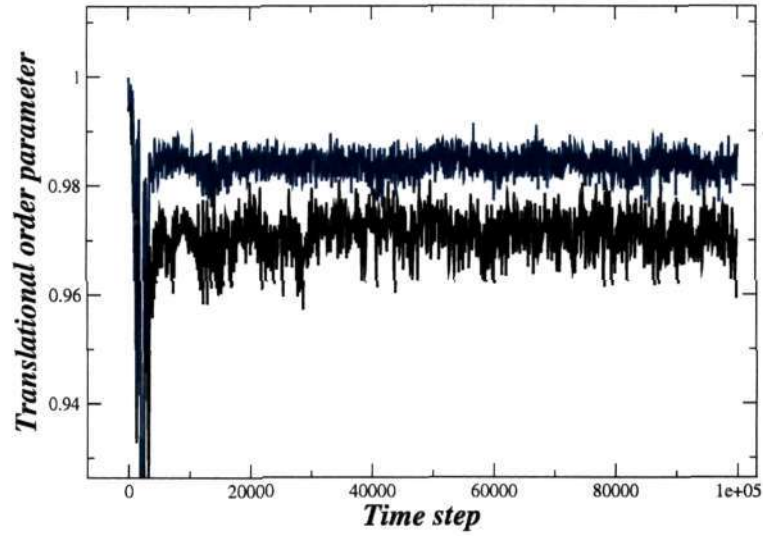
Figure 5.7: The variation of the translational order parameter of the upper wall as a function of time. The black and blue curves are respectively for the first and second upper atomic layer.
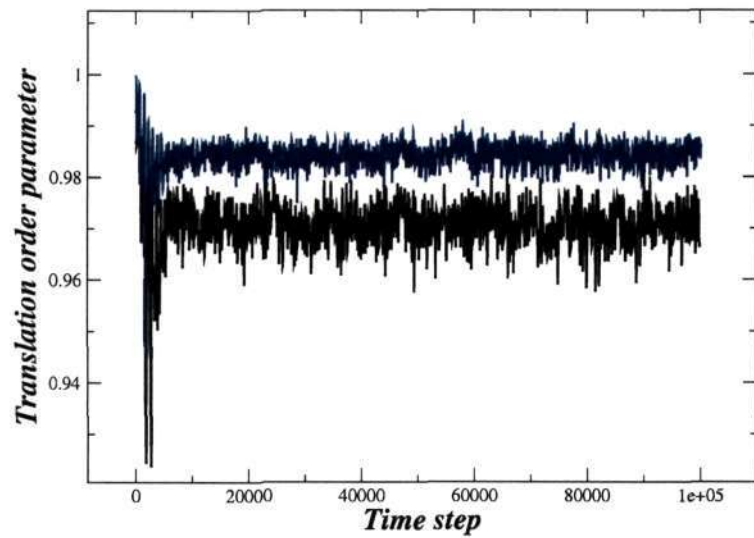
Figure 5.8: The variation of the translational order parameter as a function of time for the lower wall. The black and blue curves are respectively for the first and second lower layer.
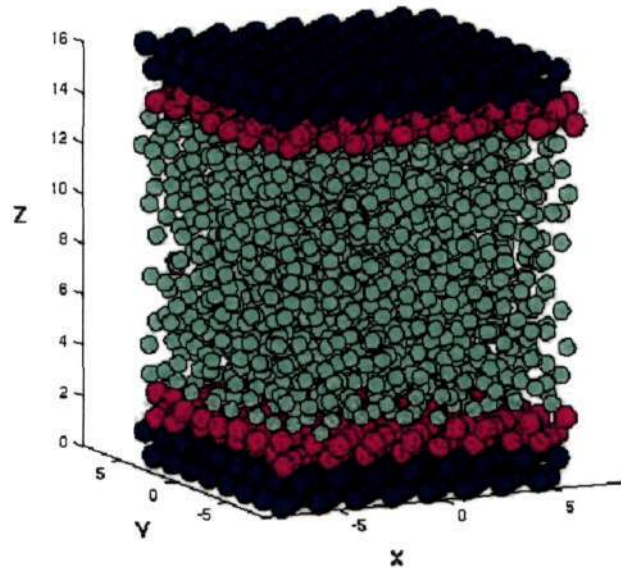
Figure 5.9: Wall-fluid configuration after equilibration, each wall consists of four atomic layers, the first two layers (magenta) are allowed to move about their mean position, the outward two layers (blue) are kept static.

at an average value during the rest of the simulation period. This average value of the order parameter is about 0.9705 for the first atomic wall layer on upper side and 0.9731 for the same on the lower side, and about 0.9844 for the second layers on both sides. These magnitudes show that the order of the wall prevails up to a good extent during the course of the simulation. A snapshot of the whole configuration is taken at the end of the simulation, which is shown in Fig. 5.9.
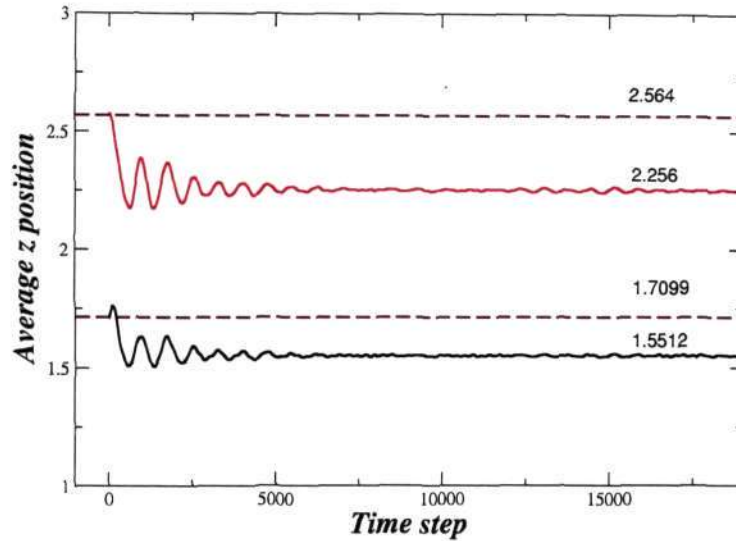
Figure 5.10: The average z position for the lower wall is shown. The dashed lines show the original wall positions and the solid lines show the the wall positions as a function of time.

In the present simulation, the first two wall-layers on both sides are found to shift in outward directions during the initial few time steps. To keep track of the wall positions, the average z position of each of the wall layers is plotted as a function of time. It is found that within about first 800 time steps, the walls on both sides move outward due to the normal hydrostatic pressure of the fluid. Then the wall position fluctuate for sometime and gradually settle down at a height where the downward pressure due to the presence of the static layers balances the fluid pressure. The amount of shift for the first wall layer is about 0.31 on both sides. Fig. 5.10, 5.11 shows the average z position as a function of time for a body force of 0.02. Navier-Stokes profile is fitted with the simulated profiles and the viscosity value is estimated for each of the body forces. The velocity profile (for a channel height of $3.78nm$) across the channel is computed by binning the particles along the z direction at threshold and below threshold acceleration, which is shown in Figs. 5.12 -
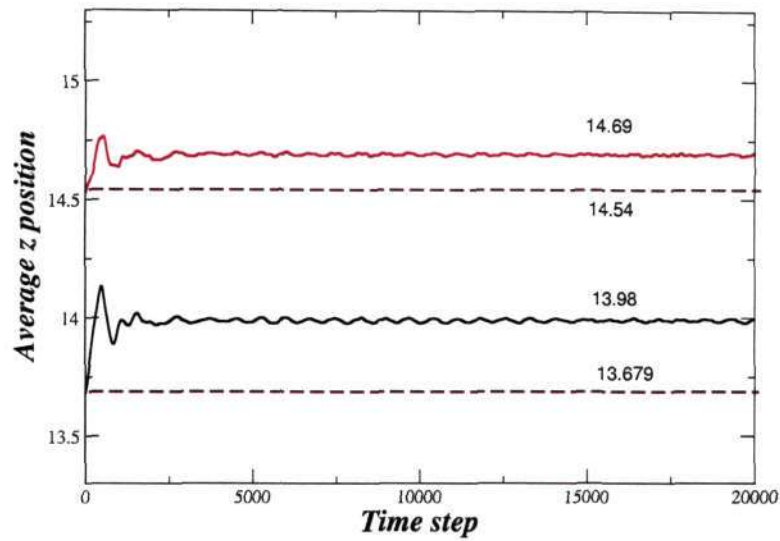
Figure 5.11: The average z position for the upper wall is shown. The dashed lines show the original wall positions and the solid lines show the wall positions as a function of time.
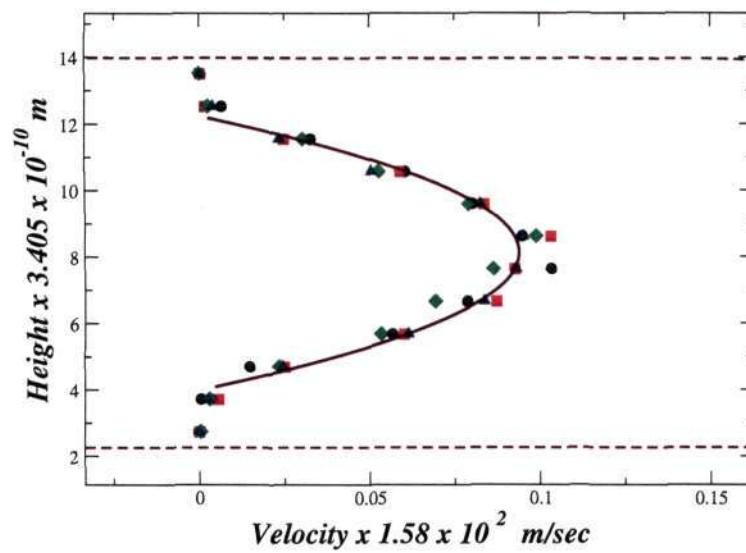
Figure 5.12: Velocity profile at a body force of 0.02. Each data set is averaged over 50000 time steps. The solid line shows a fit from the Navier-Stokes equation. The viscosity value estimated is 1.45 in reduced unit.
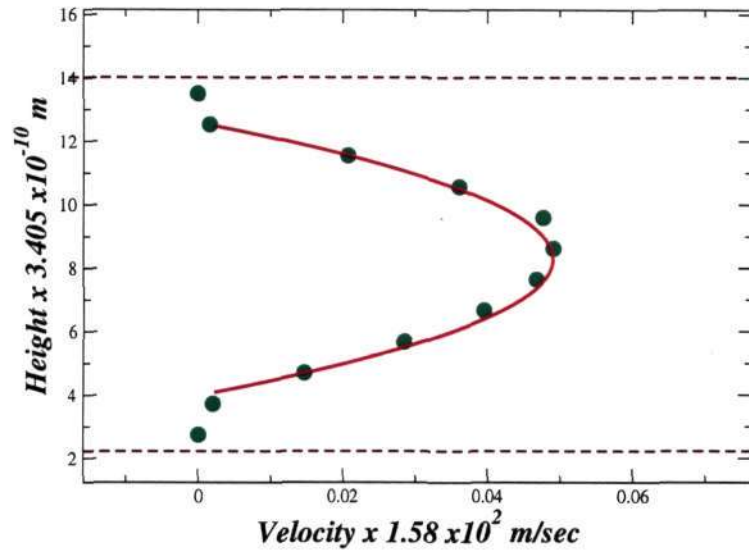
Figure 5.13: The figure shows the velocity profile at a body force of 0.01. The solid line is a fit from Navier-Stokes equation with effective wall positions $z_1 = 4.0$ and $z_2 = 12.6$ and viscosity estimated is 1.52.
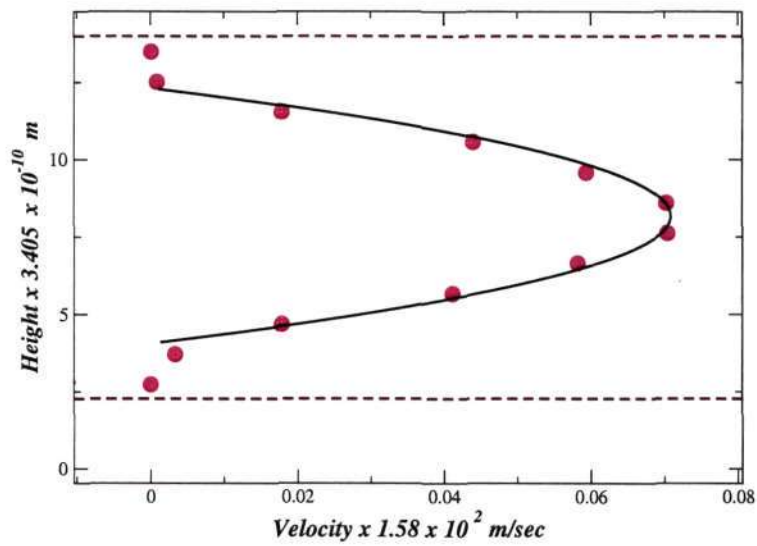
Figure 5.14: The velocity profile at a body force of 0.015. The viscosity estimated is 1.46.

5.14. 12 bins have been used and velocity profile is calculated over different blocks of 50000 time steps each after equilibration.

5.2 Calculation of viscosity by nonequilibrium molecular dynamics methods

Viscosity is independently calculated for the same state point by the method of nonequilibrium molecular dynamics. The principle is as follows. The linear response theory relates the flux J (of e.g., matter, energy, momentum) to a thermodynamic driving force or field E by the following relation.

$$J = -\kappa E \qquad (5.1)$$

where κ is the respective transport coefficient. Now if E is the shear field and J is the momentum flux, the transport coefficient connecting them is shear viscosity. The shear field is the gradient of one component of the fluid velocity, say in the x direction, with respect to another direction, say the z direction i.e, $\partial v_x/\partial z$. The momentum flux $j_z(p_x)$ is the x component of the momentum p_x transported in z direction per unit time per unit area. Following linear response theory the relation between momentum flux and gradient is given by,

$$j_z = -\eta \partial v_x/\partial z. \qquad (5.2)$$

where η is the shear viscosity. To calculate viscosity, usually a perturbation is applied in the system, the generated flux is measured and from the ratio of the two viscosity is estimated. In the present calculation a reverse procedure is employed. Here in an equilibrated liquid system an artificial flux is
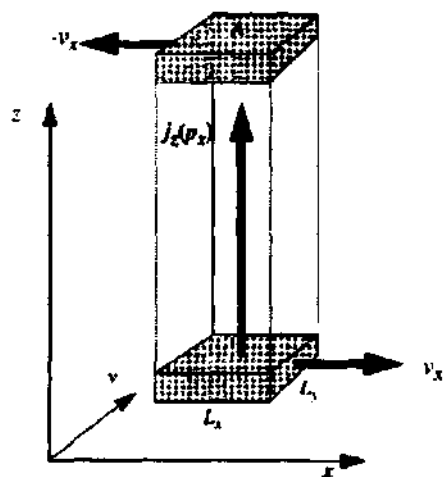
Figure 5.15: Geometry of the simulation box. A gradient in v_x is set up in the z direction by shearing the liquid. As a result, x momentum flows in the z direction, giving rise to a momentum flux j_z through the xy plane of area A.

imposed along the z direction, which causes a velocity gradient along the z direction and this velocity gradient is measured. Details of the simulation are given below. A rectangular simulation box is taken where the height in the z direction is three times that of the width with periodic boundary conditions along all the three directions as shown in the Fig. 5.15 This system is divided into 20 bins along the z direction as in Fig. 5.15 The momentum flux is imposed in an unphysical way. In the upper half of the box, the fastest moving atom in the negative x direction in the slab $z = l_z/2$ is found, similarly the fastest moving atom in the positive x direction in the slab $z = 0$ is determined. The momenta of these two atoms are then interchanged. If both atoms have the same mass this unphysical momentum swap conserves both momentum and energy. If the amount of total momentum transfer is
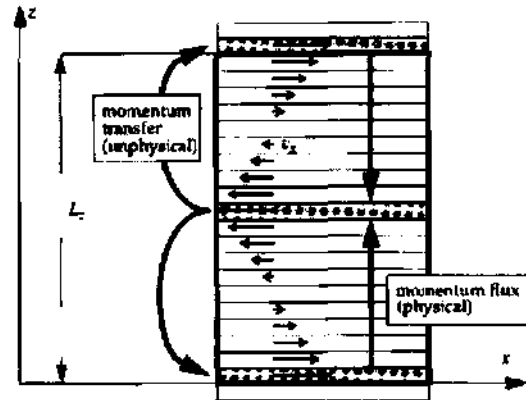
Figure 5.16: Schematic view of the periodic simulation box.

Δp_x then the momentum flux is given by

$$j_{p_x} = \Delta p_x / 2L^2 t., \qquad (5.3)$$

where L is the boxlength in x (or y) direction and t is the total simulation time. This momenta swapping between two bins is carried out periodically at a certain interval of time. Simulations are done for 1500 particles, for 150000 iteration steps, each time step taken as 0.005 and the viscosity is computed for a set of time periods of momentum exchange. Temperature of the fluid is kept fixed at 1.0 whereas density is taken as 0.8. The velocity gradient obtained is shown in Fig. 5.17.

5.3 Estimation of corrugated space and correct density

During the course of the simulation the wall layers are moving outward which changes the initial volume of the system. Consequently, the density of the
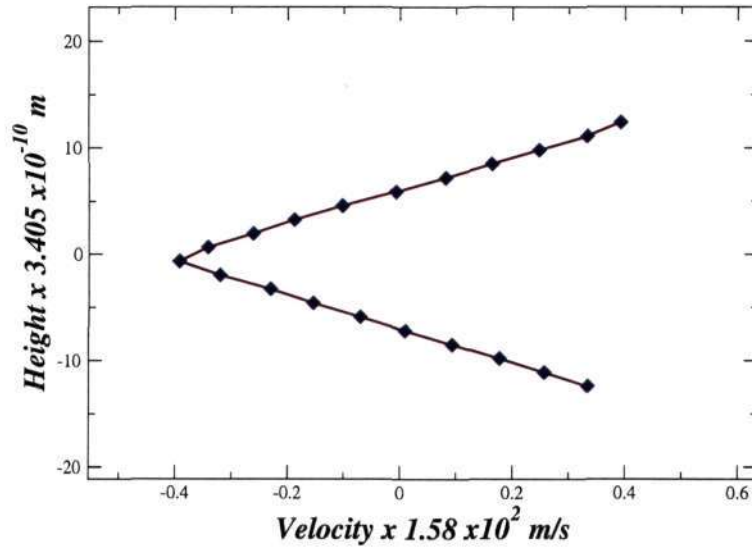
Figure 5.17: This figure shows the velocity profile across the simulation box.
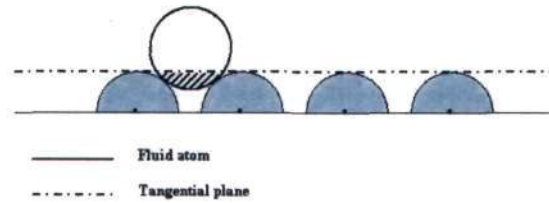
Figure 5.18: Geometrical construction, which shows the location of a near wall fluid atom with respect to the wall atoms.

system changes. There is a need to calculate the correct density of the system which requires a correct estimation of the volume of the initial system. Along with the change in volume due to the shift of the wall layers, the amount of corrugated space (due to the presence of the projected wall atom hemispheres over the surface) is also estimated to obtain the actual volume of the simulation box. The lower (or upper) wall position along z direction is taken as the z position of the tangential plane touching the projected hemispherical part of the wall atoms, as shown in Fig. 5.3. From the density
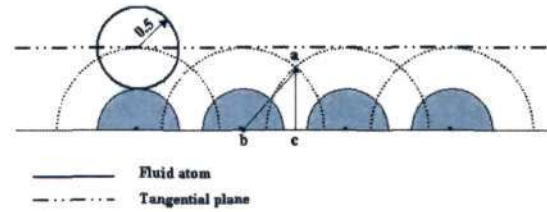
profile across the channel the first peak is found to form at a distance 0.77 away from the wall atom centers. Actually the near wall fluid atoms are sitting at the local minima of the corrugated potential surface and fluid atom centers are dipping down by a distance of 0.23 towards the wall as seen in the above figure. This distance is taken as penetration length through the above tangential plane and the excess available space for the fluid atoms is estimated by calculating the volume of the portion of the fluid atoms penetrating through this plane. This volume is in a form of a spherical cap of height 0.23 and radius same as a fluid atom (0.5). This volume is calculated and it comes out to be 17.92 which is 0.9% of the total volume. The density of the system is calculated following the above estimation and initial density found to be 0.8015 and considering the shift of the walls and the contribution of corrugated space the final density comes out to be 0.7575. The least distance between the wall and fluid atom center is 1.0 when one sits at the top of the other. According to the geometrical construction, shown in Fig. 5.3, of overlapping spheres the minimum distance(a)between wall fluid atom centers is calculated and also the excess corrugated space available for the fluid atom centers is estimated by monte carlo simulations. The least distance ab between wall and fluid atomic centers comes out to be 0.79 which is very close to the value obtained from simulation 0.77 (distance of the first peak from the wall). The volume of the corrugated space is 25.4087 which

is 1.26% of the total volume. The above analysis shows that the amount of corrugated space occupies a negligible fraction of the total volume, so does not affect the density of the system by an appreciable amount.

5.4   Comparison of viscosity

Shear viscosity of bulk fluid for the state point $\rho = 0.7575$ and temperature $T = 1.0$ is computed from the NEMD simulations and compared with the viscosity estimated from the Stokes fit of the present simulated velocity profiles. The viscosity values are also computed for the state point $\rho = 0.8$ and $T = 1.2$ which corresponds to the static wall case. Viscosity values for both the cases (static wall and wall at finite temperature) are in good agreement with the values obtained from NEMD simulations. Both the viscosity values are shown in the following tables.

Time Period	Viscosity
40	1.4926
50	1.4667
60	1.4490
70	1.5004
80	1.5142
90	1.4640
100	1.5159

Table 5.1: Viscosity data at a state point $\rho = 0.7575$ and $T = 1.0$, from NEMD simulations at different time periods of momentum swapping.

Body force	Viscosity
0.01	1.52
0.015	1.44
0.02	1.45

Table 5.2: Viscosity values at the state point $\rho = 0.7575$ and $T = 1.0$ from the Navier-Stoke's fit at different body forces at threshold and below threshold. Wall temperature is kept fixed at a value of 1.0.

Time Period	Viscosity
40	1.8712
50	1.918
60	1.8377
80	1.8006
90	1.994
100	1.987

Table 5.3: Viscosity values for the state point $\rho = 0.8$, $T = 1.2$, with static walls from NEMD simulations. Viscosity values are calculated for different time periods given in the left column.

Body force	Viscosity
0.025	1.78
0.05	2.3
0.075	1.99
0.1	1.98
0.2	1.85
0.4	1.82

Table 5.4: Viscosity values at different body forces with static wall on both sides. The state point is $\rho = 0.8$ and $T = 1.2$.

CHAPTER 6

Conclusion

In the present study, the density variation of a liquid and its flow in response to an externally applied force in a nano-sized channel has been studied by molecular dynamics simulations.

It is found that as a result of confinement the fluid density is no more uniform but displays modulations along the direction of confinement. The simulated density profiles across the channel show two distinct peaks near each wall, which indicate layering of the fluid atoms near the wall. The profiles are qualitatively the same for smooth as well as atomic wall, but the number density in the first peak is higher for the smooth wall. This is expected since the near-wall potential surface for the smooth wall is continuous whereas for the atomic wall it is corrugated with local minima, causing a lower number density. The density profile for the atomic wall agree well with Koplik & Banavar (1988). With the higher wall-fluid interaction the magnitude of near-wall peak increases and it becomes more localized.

Poiseuille flow is simulated in the system by imposing a constant body force on the fluid atoms along x direction. Thermostatting has been done in two ways, by (i) the use of an artificial thermostat with static walls (ii) allowing realistic wall-fluid interaction with walls at a fixed finite temperature. No appreciable difference in the flow properties has been observed in the two cases. In the second case, there is an upper cut off of the body force up to which the generation of heat due to the external body force is com-

63

pletely dissipated at the walls and thermal equilibration between wall and fluid is obtained. Beyond this value of body force thermal equilibration between wall and fluid is lost, but the mean fluid temperature reaches a steady state settling down at a higher value than the wall temperature. Khare *et al.* (1997) did a similar study with a shear driven flow, where the confining walls are kept at a constant temperature. They have observed significant viscous heating beyond a certain shear rate as well as the existence of non-isothermal steady temperature profiles. In the present study the binwise temperature profile for the non-isothermal case is found to be a function of z, it is higher in the center of the channel and gradually decreases from the center to the wall.

Velocity profiles are simulated for the two wall-fluid interaction strengths $e_{wf} = 1.0$ and $e_{wf} = 2.5$. It has been observed that the fluid layers immediately next to the walls get locked to the wall for both the cases and the average velocity is almost zero in these layers. In the rest of the channel a parabolic velocity profile is observed.

The Navier Stokes profile is fitted with the simulated velocity profiles and the value of the viscosity is calculated from the fitting parameters. Effective wall positions where the average velocity vanishes are obtained from such fits, and recorded as a function of the body forces. No systematic dependence of the effective wall positions on the body forces has been found. The viscosity values, for the static wall and the wall at finite temperature, estimated from the simulated velocity profiles match well with the shear viscosity value of bulk fluid calculated independently from nonequilibrium molecular dynamics simulation. The above agreement in viscosity values shows consistency with the Navier-Stokes equation.

Recently, Landman et.al studied the formation and break up of a nanojet

through molecular dynamics simulations for a range of exit orifice diameter between 2-6 nm. Their simulations show deviation from the Navier Stokes equation. The presence of the walls could have an effect in the present case. It can be inferred that more extensive study is required for the complete understanding of the flow behavior at molecular dimensions.

APPENDIX I

Reduced Unit System

The reduced unit system used in the present study and the units of all relevant physical variables in terms of M.K.S units (evaluated in terms of L-J parameters of Argon) are given in the following tables.

Basic Units	Symbol	Argon parameters
Length	σ	3.405×10^{-10}meter
Energy	ϵ	167×10^{-23} joules
Mass	m	6.626×10^{-26} kg

Variables	Reduced units	In M.K.S Units
Density	$\rho^* = \rho\sigma^3$	1680 kg/m^3
Temperature	$T^* = k_B T/\epsilon$	$119.8 K$
Viscosity	$\mu^* = \mu\sigma\tau/m$	9.076×10^{-4} poise
Pressure	$P^* = P\sigma^3/\epsilon$	41.9 Mpa
Time	$\tau^* = \left(\frac{\epsilon}{m}\sigma^2\right)^{1/2}\tau$	2.14×10^{-12}
Force	$f^* = f\frac{\sigma}{\epsilon}$	4.9×10^{-16}
Velocity	$\frac{\nu^*}{\frac{\epsilon}{m}^{1/2}}$	1.59×10^2 m/sec
Acceleration	σ/τ	$7.39 \times 10^{13} m/sec^2$

Bibliography

ABRAHAM, F. F. 1978 The interfacial density profile of a lennard-jones fluid in contact with a 100) lennard-jones wall and its relationship with idealized fluid/wall systems: A monte carlo simulation. *J. Chem. Phys.* **68(8)**, 3713.

ALLEN, M. & TILDSLEY, D. 1987 *Computer Simulation of Liquids*, 1st edn. Oxford University Press.

CHAPELA, G., SAVILLE, G., THOMPSON, S. & ROWLINSON, J. 1977 Computer simulation of a gas-liquid surface. *J.chem.soc. Faraday Trans* **73**, 1133.

CUI, CUMMINGS, P. T. & COCHRAN, H. 2001 Molecular simulation of the transition from liquidlike to solidlike behavior in complex fluids confined to nanoscale gaps. *J. Chem. Phys.* **114**, 7189.

EGGERS, J. 2002 Dynamics of nanojets. *Phys. Rev. Lett.* **89**.

FAN, X.-J., PHAN-THIEN, N., YONG, N. T. & DIAO, X. 2002 Molecular dynamics simulation of a complex nano channel flow. *Physics of fluids* **14**, 1146.

HANSEN, J. & MCDONALD, I. 1986 *The Theory of Simple Liquids*, 1st edn. Academic Press.

KHARE, R., PABLO, J. & YETHIRAJ, A. 1997 Molecular simulation and continuum mechanics study of simple fluids in non-isothermal planar couette flows. *J. Chem. Phys.* **107**, 2589.

KOPLIK, J. & BANAVAR, J. R. 1988 Molecular dynamics simulation of microscale poiseuille flow and moving contact lines. *Phys. Rev. Lett.* **60**, 1282.

KOPLIK, J. & BANAVAR, J. R. 1989 No slip condition for the mixture of two liquids. *Phys. Rev. Lett.* **80**, 5125.

LANDMANN, U. & LUEDTKE, W. D. 1991 Atomistic processes of surface and interface formation. *Appl. Surf. Sci.* **60**.

STEELE, W. A. 1973 The physical interaction of gases with crystalline soilds. *Surf. Sci.* **36**, 317–352.

THOMPSON, P. A. & ROBBINS, M. O. 1990 Shear flow near solids: Epitaxial order and flow boundary condition. *Phys. Rev. A* **41**, 6830.

ZHANG, L. & JIANG, S. 2003 Molecular simulation study of nanoscle friction between alkyl monolayers on si(111) immersed in solvents. *J. Chem. Phys.* **119**, 765.

620 . 106 4
pos